Monthly Notices
of the
ROYAL ASTRONOMICAL SOCIETY

MNRAS **460,** 1399–1416 (2016)
Advance Access publication 2016 May 6

doi:10.1093/mnras/stw1076

ETHOS – an effective theory of structure formation: dark matter physics as a possible explanation of the small-scale CDM problems

Mark Vogelsberger,[1⋆] Jesús Zavala,[2†] Francis-Yan Cyr-Racine,[3,4] Christoph Pfrommer,[5] Torsten Bringmann[6] and Kris Sigurdson[7,8]

[1]*Department of Physics, Kavli Institute for Astrophysics and Space Research, Massachusetts Institute of Technology, Cambridge, MA 02139, USA*
[2]*Dark Cosmology Centre, Niels Bohr Institute, University of Copenhagen, Juliane Maries Vej 30, DK-2100 Copenhagen, Denmark*
[3]*Department of Physics, Harvard University, Cambridge, MA 02138, USA*
[4]*California Institute of Technology, Pasadena, CA 91125, USA*
[5]*Heidelberg Institute for Theoretical Studies, Schloss-Wolfsbrunnenweg 35, D-69118 Heidelberg, Germany*
[6]*Department of Physics, University of Oslo, Box 1048, NO-0316 Oslo, Norway*
[7]*School of Natural Sciences, Institute for Advanced Study, Einstein Drive, Princeton, NJ 08540, USA*
[8]*Department of Physics and Astronomy, University of British Columbia, Vancouver, BC V6T 1Z1, Canada*

Accepted 2016 May 4. Received 2016 April 28; in original form 2015 December 21

ABSTRACT

We present the first simulations within an effective theory of structure formation (ETHOS), which includes the effect of interactions between dark matter and dark radiation on the linear initial power spectrum and dark matter self-interactions during non-linear structure formation. We simulate a Milky Way-like halo in four different dark matter models and the cold dark matter case. Our highest resolution simulation has a particle mass of $2.8 \times 10^4\,\mathrm{M}_\odot$ and a softening length of 72.4 pc. We demonstrate that all alternative models have only a negligible impact on large-scale structure formation. On galactic scales, however, the models significantly affect the structure and abundance of subhaloes due to the combined effects of small-scale primordial damping in the power spectrum and late-time self-interactions. We derive an analytic mapping from the primordial damping scale in the power spectrum to the cutoff scale in the halo mass function and the kinetic decoupling temperature. We demonstrate that certain models within this extended effective framework that can alleviate the too-big-to-fail and missing satellite problems simultaneously, and possibly the core-cusp problem. The primordial power spectrum cutoff of our models naturally creates a diversity in the circular velocity profiles, which is larger than that found for cold dark matter simulations. We show that the parameter space of models can be constrained by contrasting model predictions to astrophysical observations. For example, some models may be challenged by the missing satellite problem if baryonic processes were to be included and even oversolve the too-big-to-fail problem; thus ruling them out.

Key words: methods: numerical – galaxies: haloes – dark matter.

1 INTRODUCTION

Despite its uncertain nature, dark matter (DM) is the key driver of structure formation in the Universe. The current paradigm, the so-called cold DM (CDM) model, assumes that DM is cold and collisionless (Blumenthal et al. 1984; Davis et al. 1985). This model is extremely successful in describing the large-scale structure of the Universe (e.g. Springel 2005; Vogelsberger et al. 2014b). However, significant small-scale discrepancies on galactic and subgalactic scales remain. Specifically, (i) the problem of the abundance of dwarf galaxies, well known as the 'missing satellite (MS) problem' for galaxies in the Milky Way (MW; Klypin et al. 1999; Moore et al. 1999), and more recently pointed out also for galaxies in the field (Zavala et al. 2009; Papastergis et al. 2011; Klypin et al. 2015), (ii) the 'too-big-to-fail (TBTF) problem' (Boylan-Kolchin, Bullock & Kaplinghat 2011; Papastergis et al. 2015) and the possibly related diversity of dwarf rotation curves (Oman et al. 2015), (iii) the core-cusp (CC) problem for low surface brightness galaxies (De Blok & McGaugh 1997), and dwarf galaxies (e.g. see Oh et al. 2011; Walker & Peñarrubia 2011), and (iv) the plane of satellites problem (Pawlowski, Kroupa & Jerjen 2013).

It is at the moment unclear whether all these challenges can be fully explained within the CDM framework by invoking the complex baryonic physics in galaxy formation and evolution. However,

⋆E-mail: mvogelsb@mit.edu
† Marie Curie Fellow.

it is certain that the CDM problems are only firmly established in the discrepancies between CDM-only simulations and observations. Some of the baryonic processes that are known to happen in galaxies might actually be able to resolve these issues. Core formation, for example, might be driven by sufficiently strong supernova (SN) feedback (e.g. Navarro, Eke & Frenk 1996; Pontzen & Governato 2012; Brook & Di Cintio 2015; Chan et al. 2015; Gillet et al. 2015; Sawala et al. 2016), while gas heating during the reionization era might prevent the gas from cooling and forming stars efficiently in low-mass haloes, making them invisible to current surveys rendering the MS problem less severe. Unfortunately, there is limited evidence that can confirm if these baryonic processes can be as efficient as they need to be to become viable solutions. For instance, bursty star formation histories, occurring at shorter time-scales than the characteristic dynamical time of the galaxy, are required for SNe feedback to dramatically alter the inner DM distribution, but such time resolution is still not possible for the dwarf galaxies that show the CDM problems (Weisz et al. 2014), although there is evidence that this process is indeed efficient at larger masses (Kauffmann 2014). Furthermore, even optimistic baryonic solutions to these CDM problems fail to explain the diversity problem of dwarf galaxy rotation curves as pointed out by (Oman et al. 2015, a problem already hinted at by Kuzio de Naray et al. 2010 for LSB galaxies, see their fig. 4). On the other hand, the plane of satellites issue, could even be fully consistent with CDM in general and therefore represent no challenge to CDM (see for example Cautun et al. 2015). Regarding the abundance of dwarf galaxies, the explanation of the MS problem, which may involve a combination of observational incompleteness of current surveys and environmental processes that suppress star formation in the satellites, might not explain the dearth of field dwarfs. Here, environmental effects are likely not present – although there could be globally acting feedback like blazar heating (Pfrommer, Chang & Broderick 2012) – and surveys based on the detection of gas, such as ALFALFA, should be sensitive enough to detect most gas-bearing dwarf galaxies even if their stellar content is low. Yet, galactic winds driven by SNe explosions in galaxies with low stellar masses might well be strong enough to expel the gas from their DM haloes, and make these dwarfs invisible to cold gas surveys as well (e.g. Sawala, Scannapieco & White 2012). As this issue remains inconclusive, theoretical predictions need to be confronted with an updated census of galaxies in the local Universe (Klypin et al. 2015). It is fair to state that, at the moment, the TBTF problem, the abundance problem, the CC problem, and the diversity of dwarf galaxy rotation curves are not convincingly solved within CDM even taking into account the effects of baryons, albeit different paths towards a baryonic-only solution have been recently proposed (e.g. Brook 2015; Brook & Di Cintio 2015; Chan et al. 2015; Brook & Shankar 2016).

This motivates us to think about DM physics beyond simple CDM models, which might have a prominent role in the outstanding small-scale issues. In the CDM model, DM is assumed to be cold and collisionless. Modifications of these two basic, so far unproven DM properties, lead to differences in the non-linear structure formation process that might help to solve some of the outstanding small-scale issues of the CDM paradigm. Since the success of the CDM model needs to be preserved on large scales, one is mainly looking for small 'perturbations' around the concordant CDM model. There are mainly two alternatives studied in the context of solving galaxy formation problems that relax these hypotheses separately: warm DM (WDM) and self-interacting DM (SIDM).

While viable WDM models clearly lead to a suppression of the abundance of small haloes and a reduction of central halo densities, they do not lead to a substantial modification of the inner density profile of DM haloes, preserving the 'universal' character of the CDM Navarro–Frenk–White profile. Most importantly ∼keV thermal relic WDM does not create cores on astrophysical scales (Villaescusa-Navarro & Dalal 2011; Macciò et al. 2012), and current Lyman α forest measurements on the DM power spectrum tightly constrain thermal relics. For example, Viel et al. (2013) finds a lower limit of $m_{\rm WDM} \gtrsim 3.3\,{\rm keV}$, which is too large to provide solutions to the small-scale problems of CDM that require $m_{\rm WDM} \sim 2\,{\rm keV}$ (Schneider et al. 2014). Nevertheless, even modest small-scale modifications of the initial power spectrum lead to effects on the satellite population of haloes, that are interesting in the context of the MS problem. Thermal relic WDM is most likely not the right idea to provide these modifications in a way consistent with current observations and constraints (although see the recent analysis by Garzilli et al. 2015, which relaxes the Viel et al. 2013 constraints significantly). There might exist some so far unexplored viable WDM models (e.g. sterile neutrinos Boyarsky et al. 2009), but only a few *N*-body simulations with these models have been done (e.g. Lovell et al. 2012).

On the other hand, the internal mass distribution of DM haloes can be modified substantially in allowed SIDM models, forming density cores through an effective inwards heat flux that drives haloes towards an isothermal configuration. If the self-scattering cross-section per unit mass is $\sim 1\,{\rm cm^2\,g^{-1}}$ at the scale of dwarf galaxies, SIDM models can solve both the CC and TBTF problems (Vogelsberger, Zavala & Loeb 2012; Rocha et al. 2013; Zavala, Vogelsberger & Walker 2013). In SIDM, the (sub)halo abundance can potentially be modified as well if the cross-section is large enough, which was one of the original motivations of the SIDM model (Spergel & Steinhardt 2000). However, the cross-sections required for this to happen are seemingly too large, of $\mathcal{O}(10\,{\rm cm^2\,g^{-1}})$ on galactic scales, clearly above the most up-to-date constraints, which suggest that constant cross-sections larger than $1\,{\rm cm^2\,g^{-1}}$ are ruled out (Peter et al. 2013). At the level of these bounds, there are no significant differences between the SIDM and CDM (sub)halo abundances (Vogelsberger et al. 2012; Rocha et al. 2013). It is important to recall however, that such conclusions are based on DM-only simulations. Recent analytical estimates suggest that the constraints might get weaker once the effects of baryons are considered (Kaplinghat et al. 2014). Additionally, since current constraints are all beyond the scale of massive ellipticals (see however Kaplinghat, Tulin & Yu 2016, for some model dependent constraints on other mass scales, which point to a slight velocity dependence of the cross-section), the possibility remains that DM has very large cross-section on smaller (dwarf-size) scales, dropping below current bounds at larger scales. This velocity-dependent cross-section is also the natural outcome of many particle physics models of SIDM (e.g. Ackerman et al. 2009; Feng et al. 2009; Feng, Kaplinghat & Yu 2010; Buckley & Fox 2010; Loeb & Weiner 2011). On the observational side, Massey et al. (2015) recently found an offset between the inferred position of the DM halo and the stars of one of the four bright cluster galaxies in the 10 kpc core of Abell 3827. This offset could be interpreted as potential evidence for SIDM with a cross-section of $\sim 1.5\,{\rm cm^2\,g^{-1}}$ (Kahlhoefer et al. 2015), in marginal tension with current constraints. Although such an offset might be caused by astrophysical effects unrelated to the DM nature, its amplitude appears to be extremely rare within the CDM model (Schaller et al. 2015).

We note that the SIDM and WDM models explored in the context of structure formation are just a subgroup of a broader class of possible alternative DM models. To mention a couple of less

explored models, DM from late decays (Sigurdson & Kamionkowski 2004; Kaplinghat 2005; Borzumati, Bringmann & Ullio 2008), and extremely light DM forming condensates (Hu, Barkana & Gruzinov 2000; Peebles 2000) with particle masses of the order of 10^{-22} eV. The latter class of models is particularly interesting since non-QCD axions could be a potential candidate for such light DM, which would be described by a single coherent wavefunction (see Schive, Chiueh & Broadhurst 2014, for some simulation results).

We would like to stress that all these different modifications to the CDM paradigm are also motivated by the fact that the most simple CDM candidates (weakly interacting massive particles, WIMPs) have not been discovered despite decades long efforts (e.g. Bertone, Hooper & Silk 2005; Bertone 2010). Furthermore, there has also been no sign of Supersymmetry at the LHC so far, which has provided a strong theoretical support for several excellent CDM-WIMP candidates like the neutralino (Jungman, Kamionkowski & Griest 1996). Based on these null results, the time is ripe to think beyond simple CDM models. The fact that some of these alternative models can actually also solve astrophysical problems with CDM should be seen as a motivation to go beyond the purely particle physics based considerations. In the end there is also no compelling reason for the fact that the dark sector should be dominated by a single featureless WIMP particle only. After all, the visible sector is very rich, and this might also be true for the dark sector. From the perspective of structure formation, the CDM model is only an effective description that assumes that the only DM interaction that matters is gravity. Since such an assumption remains unverified, it is crucial that we develop a more generic effective framework that includes a broad range of allowed DM interactions.

SIDM simulations have so far mainly considered the late-time impact of DM collisions, i.e. those simulations started with a CDM transfer function and implemented some form of scattering (mostly elastic and isotropic, but see Medvedev 2014 and Randall & Scholtz 2015 for first approaches going beyond this) of DM particles, which then affects the non-linear structure formation process. Under these conditions, SIDM simulations have shown that DM collisions can hardly affect the abundance of dwarf-size haloes without violating current constraints on the cross-section. This has led to the impression that SIDM by itself is not able, for example, to solve or alleviate the CDM problem on the abundance of dwarf galaxies (Brooks 2014). However, most previous SIDM simulations neglect the possibility of modifying the primordial linear power spectrum. Although DM self-collisions are not strong enough to impact the power spectrum on galactic scales, additional interactions with relativistic particles (e.g. photons or dark radiation) in the early Universe can suppress the formation of dwarf-scale haloes (Bœhm et al. 2002, 2014; Buckley et al. 2014). This can in fact be naturally accommodated in SIDM models, for exactly the range of parameters that address the TBTF and the CC problem, by allowing the vector field that mediates DM self-interactions to also couple to (sterile) neutrinos or any other form of dark radiation (DR; Van den Aarssen, Bringmann & Pfrommer 2012; Bringmann, Hasenkamp & Kersten 2014; Dasgupta & Kopp 2014). The result is a much later kinetic decoupling of DM than in the standard case (Bringmann 2009), leading to cutoff scales of the primordial linear power spectrum that are on mass scales of the order of dwarf galaxies and hence alleviate the overabundance problem of these (sub)haloes in CDM cosmologies (Van den Aarssen et al. 2012; Bœhm et al. 2014; Buckley et al. 2014; Schewtschenko et al. 2015). In general, this suppression of the initial power spectrum has a similar impact in structure formation as that seen in vastly studied WDM simulations, but with more complex features that create richer possibilities. Depending on the detailed particle physics model, the power spectrum can have some non-trivial features like dark acoustic oscillations (DAOs) and a Silk damping tail (e.g. Buckley et al. 2014), which are a general phenomena of e.g. atomic DM models (e.g. Cyr-Racine & Sigurdson 2013). Such features are not present in thermal WDM where the power spectrum suppression is driven by the free streaming of DM particles mainly resulting in a pure exponential cutoff. It is however important to mention that *N*-body simulations with DAO-like features in the power spectrum have been explored in the past in the context of different particle physics models, e.g. the consequences for the abundance of (sub)haloes in models with long-lived charged massive particles were explored in Kamada et al. (2013).

Virtually all previous SIDM simulations have neglected the combined effect of modifications to the initial power spectrum due to DM interactions with relativistic particles and DM collisions due to DM self-scattering. There is no single cosmological simulation that considers a SIDM model, where the initial power spectrum and self-interactions are consistently chosen. A first attempt in this direction was made very recently by Buckley et al. (2014), but this work did not take into account the proper velocity dependence of the scattering cross-section, assuming instead a constant cross-section. We present here the first *N*-body simulations where viable particle physics models are used as an input to compute the initial power spectrum (strongly modified by DM-DR interactions) and the velocity dependent DM–DM cross-section. Our models have therefore three main features that affect structure formation: (i) a suppression of primordial structure due to a Silk-like damping mechanism, (ii) an imprint of DAOs in the initial matter power spectrum (driven by DM-DR interactions), and (iii) a modification of DM halo properties due to the self-interaction of DM in the non-linear regime of structure formation. We will demonstrate that such features have interesting effects on the abundance and the internal structure of haloes and subhaloes, and thereby successfully address most of the current small-scale issues of CDM.

For a significant fraction of such DM models, the amplitude and shape of the initial linear matter power spectrum, and the size of the self-interaction cross-section at different velocities largely determine the abundance and structure of DM haloes on a variety of mass scales. Therefore, distinct DM particle models that make similar predictions for the linear matter power spectrum and self-interaction cross-section, can be classified into a single 'effective theory of structure formation' (ETHOS). This is useful since all DM particle models that map to a given effective theory can be simultaneously constrained by comparing a single ETHOS numerical simulation to observations at no extra cost or effort. This ETHOS framework aims at generalizing the theory of DM structure formation to include a wide range of allowed DM phenomenology (see Cyr-Racine et al. 2015, for details). The goal of this work is to explore a few ETHOS benchmark cases and demonstrate their interesting behaviour at the scale of galactic subhaloes. We will also demonstrate that the parameter space of these models can actually be constrained by astrophysical observations; for example, in cases that lead to an unrealistic reduction of substructure in galactic haloes, or inner density profiles that are too low compared to astrophysical constraints.

This paper has the following structure. We present the different ETHOS models discussed in this work in Section 2, where we present their particle physics parameters and their mapped initial linear power spectra and cross-sections. We introduce in total four different ETHOS models. Section 3 discusses the different simulations carried out to explore these models. Here we describe

our uniform box and zoom-in simulations. The results of these simulations are then presented in Section 4, where we first focus on general results based on the uniform box simulations before discussing the structure of the galactic halo within the different models. In this section we will also try to construct a model which solves some of the outstanding small-scale problems of the MW satellites. Finally, we present our summary and conclusions in Section 5.

2 EFFECTIVE MODELS

The different DM models that we investigate in this paper are summarized in Table 1. For all simulations we use the following cosmological parameters: $\Omega_{\rm m} = 0.302$, $\Omega_\Lambda = 0.698$, $\Omega_{\rm b} = 0.046$, $h = 0.69$, $\sigma_8 = 0.839$, and $n_s = 0.967$, which are consistent with recent Planck data (Planck Collaboration XVI 2014; Spergel, Flauger & Hložek 2015). We study mainly five different DM models, which we label CDM and ETHOS-1 to ETHOS-4. In the parameter space of ETHOS, these models are represented by a specific transfer function (see left-hand panel of Fig. 1 for the resulting linear dimensionless power spectra), and a specific velocity-dependent transfer cross-section for DM (see right-hand panel of Fig. 1). Our discussion will mostly focus on ETHOS-1 to ETHOS-3, which demonstrate the basic features of our ETHOS models. ETHOS-4 is a tuned model that was specifically set up to address the small-scale issues of CDM (the MS problem and the TBTF problem). We discuss this model towards the end of the paper.

These models arise within the effective framework of ETHOS, described in detail in Cyr-Racine et al. (2015), which we summarize

Table 1. Parameters of the effective DM models considered in this paper. We study in total five different scenarios (CDM and models ETHOS-1 to ETHOS-4). ETHOS models are characterized by four intrinsic parameters: the coupling between the mediator and DM ($\alpha_\chi \equiv g_\chi^2/4\pi$), the coupling between the mediator and a massless neutrinos-like fermion ($\alpha_\nu \equiv g_\nu^2/4\pi$), the mediator mass ($m_\phi$), and the mass of the DM particle (m_χ). In principle, the ratio of neutrino-like fermion and photon temperature constitutes another parameter that follows from the underlying particle physics framework; for definiteness, we will set it throughout to 0.5 in this paper. ETHOS models are characterized by five effective parameters (see equations 1 and 2): a_4 and $\alpha_{l\geq 2} = 3/2$ (constant for these models and thus absent from the table), which determine the linear power spectrum (left-hand panel of Fig. 1), while the velocity dependence of the DM self-interaction cross-section (right-hand panel of Fig. 1) is described by three characteristic cross-sections at three different velocities (30, 200, 1000 km s^{-1}). As a reference, we also provide two characteristic comoving length scales: the DM sound horizon ($r_{\rm DAO}$), and the Silk damping scale ($r_{\rm SD}$). ETHOS-4 is a tuned model that was specifically set up to address some of the small-scale issues of CDM (the MS problem and the TBTF problem).

Name	α_χ	α_ν	m_ϕ (MeV c^{-2})	m_χ (GeV c^{-2})	$r_{\rm DAO}$ (h^{-1} Mpc)	$r_{\rm SD}$ (h^{-1} Mpc)	a_4 (h Mpc^{-1})	$\langle\sigma_T\rangle_{30}/m_\chi$ (cm^2 g^{-1})	$\langle\sigma_T\rangle_{200}/m_\chi$ (cm^2 g^{-1})	$\langle\sigma_T\rangle_{1000}/m_\chi$ (cm^2 g^{-1})
CDM	–	–	–	–	–	–	–	–	–	
ETHOS-1	0.071	0.123	0.723	2000	0.362	0.225	14 095.65	4.98	0.072	0.0030
ETHOS-2	0.016	0.03	0.83	500	0.217	0.113	1784.05	9.0	0.197	0.000 97
ETHOS-3	0.006	0.018	1.15	178	0.141	0.063	305.94	16.9	0.48	0.0028
ETHOS-4 (tuned)	0.5	1.5	5.0	3700	0.138	0.0615	286.09	0.16	0.022	0.000 75

Note. CDM: has MS and TBTF problems, ETHOS-1: oversolves MS and TBTF problems, ETHOS-2: oversolves TBTF problem, ETHOS-3: oversolves TBTF problem, ETHOS-4 (tuned): alleviates MS and TBTF problems.

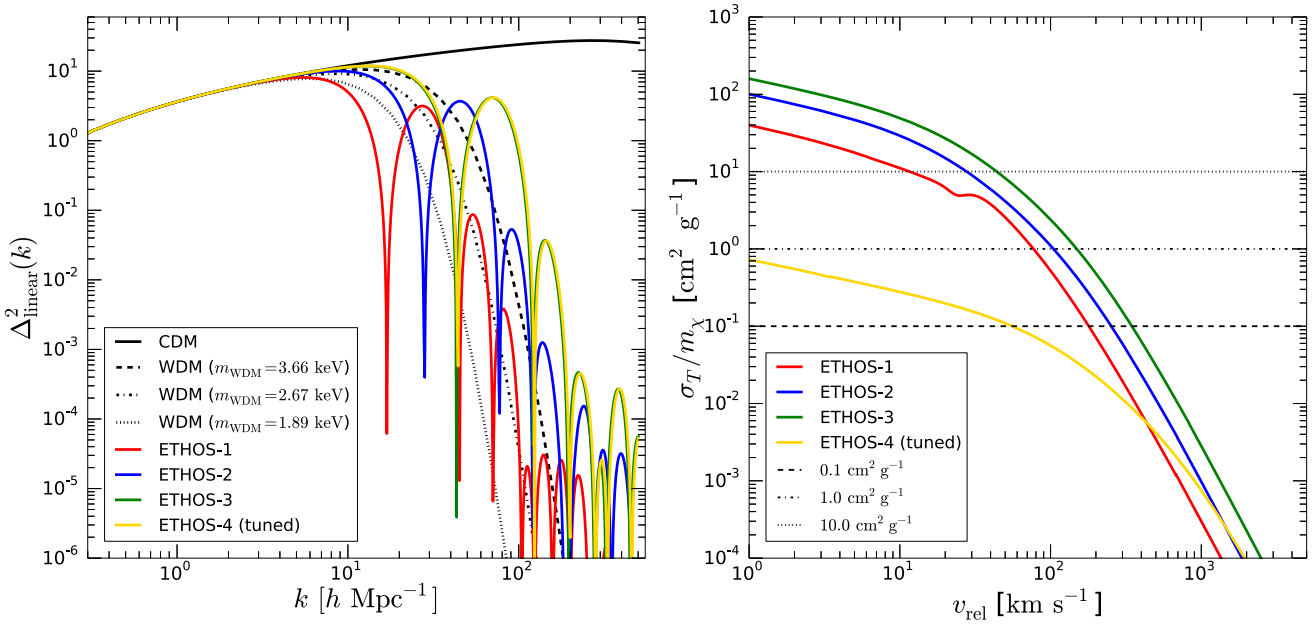

Figure 1. Properties of the effective DM models relevant for structure formation. Left: linear initial matter power spectra ($\Delta_{\rm linear}(k)^2 = k^3 P_{\rm linear}(k)/2\pi^2$) for the different models (CDM and ETHOS models ETHOS-1 to ETHOS-4) as a function of comoving wavenumber k. The ETHOS models differ in the strength of the damping and the DAOs at small scales. As a reference, we also include thermal-relic-WDM models, which are close to each model in ETHOS. Right: velocity dependence of the transfer cross-section per units mass (σ_T/m) for the different ETHOS models. Models ETHOS-1 to ETHOS-3 have $\sigma_T/m \propto v_{\rm rel}^{-4}$ for large relative velocities. For low velocities, the cross-sections can be as high as 100 cm^2 g^{-1}.

in the following. ETHOS provides a mapping between the intrinsic parameters (couplings, masses, etc.) defining a given DM particle physics model, and (i) the effective parameters controlling the shape of the linear matter power spectrum, and (ii) the effective DM transfer cross-section ($\langle\sigma_T\rangle/m_\chi$); both at the relevant scales for structure formation. Schematically:

$$\begin{aligned}\{m_\chi, \{g_i\}, \{h_i\}, \xi\} &\rightarrow \{\omega_{\rm DR}, \{a_n, \alpha_l\}, \{b_n, \beta_l\}, \{d_n, m_\chi, \xi\}\} \\ &\rightarrow P_{\rm lin,matter}(k) \\ \{m_\chi, \{h_i\}, \{g_i\}\} &\rightarrow \left\{\frac{\langle\sigma_T\rangle_{30}}{m_\chi}, \frac{\langle\sigma_T\rangle_{220}}{m_\chi}, \frac{\langle\sigma_T\rangle_{1000}}{m_\chi}\right\}, \end{aligned} \quad (1)$$

where the parameters on the left are the intrinsic parameters of the DM model: m_χ is the mass of the DM particle, $\{g_i\}$ represents the set of coupling constants, $\{h_i\}$ is a set of other internal parameters such as mediator mass and number of degrees of freedom, and $\xi = (T_{\rm DR}/T_{\rm CMB})|_{z=0}$ is the present-day DR to CMB temperature ratio.

The effective parameters of the framework are on the right of equation (1), which in all generality include the cosmological density of DR $\omega_{\rm DR} \equiv \Omega_{\rm DR}h^2$, the set $\{a_n, \alpha_l\}$ characterizing the DM-DR interaction, the $\{b_n, \beta_l\}$ set characterizing the presence of DR self-interaction (relevant, for instance, to non-abelian DR), and the parameter set $\{d_n, m_\chi, \xi\}$ determining the evolution of the DM temperature and adiabatic sound speed. This latter quantity is very small for non-relativistic DM, and it has thus little impact on the evolution of linear DM perturbations (except on very small scales, irrelevant for galaxy formation/evolution). In this work, we focus our attention on the effect of DM-DR interaction on the evolution of DM perturbations. The physics of these effects are captured by the parameters $\{a_n, \alpha_l\}$, where the set of l-dependent coefficients α_l encompasses information about the angular dependence of the DM-DR scattering cross-section, whereas the a_n are the coefficients of the power-law expansion in temperature (redshift) of the DM drag opacity caused by the DM-DR interaction (see section II E of Cyr-Racine et al. 2015). Physically, a single non-vanishing a_n implies that the squared matrix element for the DM-DR scattering process scales as $|\mathcal{M}|^2 \propto (p_{\rm DR}/m_\chi)^{n-2}$, where $p_{\rm DR}$ is the DR momentum. We leave the impact of DR self-interactions on the matter power spectrum to a future study. We note that DR self-interaction as parametrized by $\{b_n, \beta_l\}$ can actually have a non-negligible effect on the linear matter power spectrum through its influence on the gravitational shear stress. However, this latter effect is generally subdominant compared to the DM-DR interactions studied in this work.

The other set of effective parameters in ETHOS are related to DM self-scattering. Although each particle physics model would have a specific transfer cross-section, in ETHOS we classify (characterize) a given model based on the values of its cross-section at three relative velocities, those characteristic of dwarf galaxies ($\sim$30 km s^{-1}), the MW-size galaxies ($\sim$220 km s^{-1}) and galaxy clusters ($\sim$1000 km s^{-1}).[1] The choice of these three characteristic velocities is arbitrary but it allows us at a glance to (i) check whether a given model is compatible with observations, and (ii) have a reliable estimate at what the outcome of the simulation of a given model would be based on the results of models already simulated, which have similar values of the transfer cross-section. For instance, if two models have the same values of $\langle\sigma_T\rangle_{30}/m_\chi$, full simulations of isolated dwarfs in each model are likely to yield similar results, even though they might have very different values of $\langle\sigma_T\rangle_{1000}/m_\chi$. Furthermore, these characteristic velocities mark also three relevant regimes for any model containing DM self-interactions: (i) the dwarf-scale regime where the CDM model is being challenged, and where the transfer cross-section is largely unconstrained, (ii) the intermediate-scale regime where a large cross-section can lead to the evaporation of subhaloes in MW-size galaxies, and (iii) the cluster-scale regime where observations put the strongest constraints to the cross-section.

The ETHOS framework described above is general, but for the purpose of this work we restrict ourselves to an underlying particle physics model which assumes, like in Van den Aarssen et al. (2012), a massive fermionic DM particle (χ) interacting with a massless neutrino-like fermion (ν) via a massive vector mediator (ϕ). This model is characterized by an interaction between DM and DR and DM-DM self-interactions (see section II F.1 of Cyr-Racine et al. 2015, for details). The former gives rise to the features in the power spectrum, which are absent in ordinary CDM transfer functions, while the latter alters the evolution of DM haloes across time. This model is characterized by a squared matrix element scaling as $(p_{\rm DR}/m_\chi)^2$, which immediately implies that the impact of DM-DR scattering on the linear matter power spectrum is entirely captured by a non-vanishing a_4 coefficient. For DM-DR interactions leading to late kinetic decoupling, this is indeed a very commonly encountered situation according to a recent comprehensive classification of such scenarios Bringmann et al. (2016); note, however, that in the presence of *scalar* mediators it is sometimes rather a_2 that is the only non-vanishing coefficient a_n (depending on the spin of DM and DR).

In our case, the ETHOS mapping is reduced to

$$\{m_\chi, m_\phi, g_\chi, g_\nu, \eta_\chi, \eta_\nu, \xi\} \longrightarrow \left\{\omega_{\rm DR}, a_4, \alpha_{l\geq 2} = \frac{3}{2}, \frac{\langle\sigma_T\rangle_{30}}{m_\chi}, \frac{\langle\sigma_T\rangle_{220}}{m_\chi}, \frac{\langle\sigma_T\rangle_{1000}}{m_\chi}\right\}. \quad (2)$$

The model is characterized by six intrinsic particle physics parameters: the mass of the DM particle (m_χ), the mediator mass (m_ϕ), the coupling between the mediator and DM (g_χ), the coupling between the mediator and neutrino-like fermions (g_ν), the number of DM spin states (η_χ), and the number of spin states of the neutrino-like fermion (η_ν). In principle, the ratio of neutrino-like fermion and photon temperature ξ constitutes another parameter that follows from the underlying particle physics framework; for definiteness, we will set it throughout to 0.5 in this work. The effective ETHOS parameters that fully characterize the linear power spectrum are then reduced to three: the abundance of DR $\omega_{\rm DR}$, the opacity parameter a_4 ($a_{n\neq 4} = 0$), and a set of constant $\alpha_{l\geq 2}$ values. It is possible to calculate these parameters analytically (Cyr-Racine et al. 2015)

$$\begin{aligned} a_4 &= (1+z_{\rm D})^4 \frac{\pi g_\chi^2 g_\nu^2}{m_\phi^4} \frac{\tilde{\rho}_{\rm crit}}{m_\chi} \left(\frac{310}{441}\right) \xi^2 T_{\rm CMB,0}^2, \\ \alpha_{l\geq 2} &= \frac{3}{2}, \end{aligned} \quad (3)$$

where $\tilde{\rho}_{\rm crit} \equiv \rho_{\rm crit}/h^2$ with $\rho_{\rm crit}$ the critical density of the Universe, and $T_{\rm CMB,0}$ is the temperature of the CMB today. The normalization redshift $z_{\rm D}$ is arbitrary, but choosing it to be the redshift of DM kinetic decoupling ensures that the a_n coefficients are generally of order unity. For models that modify the linear matter power spectrum on subgalactic scales, we usually have $z_{\rm D} \gtrsim 10^7$. The generic form of the a_4 coefficient is easy to understand: the combination $g_\chi^2 g_\nu^2/m_\phi^4$ is the leading factor in the squared scattering

[1] Note that in some cases one needs to go beyond the transfer cross-section to describe the effect of self-interactions, see e.g. Kahlhoefer et al. (2014).

amplitude, the term $\tilde{\rho}_{\rm crit}/m_\chi$ is proportional to the DM number density, and the remaining factors come from thermally averaging $p_{\rm DR}^2$ over the Fermi–Dirac distribution describing the DR phase-space. The non-unity value of the angular coefficients $\alpha_{l\geq 2}$ is caused by the angular dependence of the DM-DR scattering cross-section which scales as $1+\cos\theta$, where θ is the angle between the outgoing DM and DR particles.

The other set of effective parameters are those related to the velocity-dependent DM self-interaction cross-section expected for a Yukawa potential between the DM particles (given the choice of particle physics model; see e.g. Loeb & Weiner 2011), evaluated at the three characteristic velocities of the ETHOS framework. The formula for the DM momentum transfer cross-section has been obtained in analogy with the screened Coulomb scattering in a plasma (see the improved equations 100 and 101 in Cyr-Racine et al. 2015). Most importantly, the behaviour of the cross-sections is to fall off rapidly towards large relative velocities. It is therefore possible to have large cross-sections at small scales (i.e. low relative velocities, for example at the dwarf scale) while at the same time satisfy constraints on cluster scales.

Table 1 specifies the relevant particle physics and effective parameters for the cases we have simulated in this work. The effective parameters that control the shape of the linear power spectrum are related to more familiar scales in the initial power spectrum: the comoving diffusion (Silk) damping scale ($r_{\rm SD}$) and the DM comoving sound horizon ($r_{\rm DAO}$). These are generic scales, which occur in models where DM is coupled to relativistic particles in the early Universe, i.e. they are not only a consequence of the specific particle physics scenario used here. Currently, or simulations only cover the regime for which $r_{\rm DAO} \gtrsim r_{\rm SD}$ ('weak' DAOs); for an example of a simulation in the strong DAOs regime, with $r_{\rm DAO} \gg r_{\rm SD}$, see Buckley et al. (2014).

As a reference, the left-hand panel of Fig. 1 also shows three WDM power spectra for thermal relics, which are described by a sharp cutoff (we follow Bode, Ostriker & Turok 2001, with $\nu = 1$):

$$P_{\rm WDM}(k) = T^2(k) P_{\rm CDM}(k), \quad T(k) = (1+(\alpha k)^2)^{-5}, \tag{4}$$

where the α parameter defines the cutoff scale in the initial power spectrum and is related to the free streaming of WDM particles. The α value can be associated with a generic thermal relic WDM particle mass, $m_{\rm WDM}$, using the relation (Bode et al. 2001):

$$\alpha = \frac{0.05}{h\,{\rm Mpc}^{-1}} \left(\frac{m_{\rm WDM}}{1\,{\rm keV}}\right)^{-1.15} \left(\frac{\Omega_{\rm WDM}}{0.4}\right)^{0.15} \left(\frac{h}{0.65}\right)^{1.3} \left(\frac{g_{\rm WDM}}{1.5}\right)^{-0.29}, \tag{5}$$

where $\Omega_{\rm WDM}$ is the WDM contribution to the density parameter, and $g_{\rm WDM}$ the number of degrees of freedom. It is conventional to use 1.5 as the fiducial value for $g_{\rm WDM}$ for the WDM particle. The left-hand panel of Fig. 1 shows also the WDM particle masses for the three cases, which were chosen by eye to match the initial power decline of the ETHOS models as well as the friend-of-friends (FoF) halo mass function (see Fig. 3 and discussion further down).

We note that the Lyman α forest is sensitive to any sort of small-scale cutoffs in the power spectrum; a feature that puts, for example, tight constraints on the mass of thermal-relic-WDM particles (Viel et al. 2013). The acoustic oscillation ($r_{\rm DAO}$) and damping ($r_{\rm SD}$) scales can therefore, in principle, be constrained via Lyman α forest data as well. Since the shape of the cutoff in our models is very different from the exponential cutoff in WDM models, it is thus necessary to perform detailed hydrodynamical simulations for the models presented here in order to obtain appropriate Lyman α forest constraints. We will discuss this in a forthcoming work (Zavala et al. in preparation).

3 SIMULATIONS

We generate initial conditions at $z = 127$ within a $100\,h^{-1}$ Mpc periodic box (our parent simulation) from which we select a MW-size halo to be resimulated with a zoom technique. The transfer functions for all DM models were generated with a modified version of the CAMB code (Seljak & Zaldarriaga 1996; Lewis & Challinor 2011), as described in Cyr-Racine et al. (2015). All initial conditions were generated with the MUSIC code (Hahn & Abel 2011). The uniform parent simulation is performed at a resolution of 1024^3 particles yielding a DM particle mass resolution of $7.8 \times 10^7\,h^{-1}\,{\rm M}_\odot$ and a spatial resolution (Plummer-equivalent softening length) of $\epsilon = 2\,h^{-1}$ kpc. This is sufficient to resolve haloes down to $\sim 2.5 \times 10^9\,h^{-1}\,{\rm M}_\odot$ with about 32 particles. We note that the mass and spatial resolution of this parent simulation is slightly better than the simulations presented in Buckley et al. (2014), which have a smaller simulation volume. The parent simulation presented here has therefore better statistics and also includes more massive clusters. It contains 10 haloes with a virial mass ($M_{200,\,\rm crit}$) above $10^{14}\,h^{-1}\,{\rm M}_\odot$ at $z = 0$.

The galactic halo for resimulation was randomly selected from a sample of haloes that have masses between $1.58 \times 10^{12}\,{\rm M}_\odot$ and $1.61 \times 10^{12}\,{\rm M}_\odot$, which is in the upper range of current estimates for the mass of the MW halo (see fig. 1 of Wang et al. 2015). This sample was created using only those MW-size haloes which do not have another halo more massive than half their masses within $2\,h^{-1}$ Mpc (this is a criterion for isolation). We stress that we do not consider a Local Group analogue here in this first study. We have simulated the selected halo at three different resolutions, level-3 to level-1, which are summarized in Table 2. For these resimulations, the softening length is fixed in comoving coordinates until $z = 9$, and is then fixed in physical units until $z = 0$. The latter value is quoted in Table 2. The number of high-resolution particles refers to the CDM simulation only; the other DM models produce slightly different numbers. The most basic characteristics of the halo are presented in Table 3 for the highest resolution simulations.

Self-scattering of DM particles was implemented into the AREPO code (Springel 2010) following the probabilistic approach described in Vogelsberger et al. (2012), which assumes that scattering is elastic and isotropic. This implementation has previously been used, in the context of standard SIDM (i.e. with the same power spectrum as CDM), to constrain the self-interaction cross-section at the scale of the MW dwarf spheroidals (Zavala et al. 2013), predict direct detection signatures of self-interactions (Vogelsberger & Zavala 2013), and study the impact on lensing signals (Vegetti & Vogelsberger

Table 2. Simulation parameters of the selected MW-size halo. We list the DM particle mass ($m_{\rm DM}$), the Plummer-equivalent softening length (ϵ), and the number of high-resolution particles ($N_{\rm hr}$). The softening length is kept fixed in physical units for $z < 9$. The number of high-resolution particles refers to the CDM case and slightly varies for the other DM models.

Name	$m_{\rm DM}$ (${\rm M}_\odot$)	ϵ (pc)	$N_{\rm hr}$
level-1	2.756×10^4	72.4	444 676 320
level-2	2.205×10^5	144.8	55 451 880
level-3	1.764×10^6	289.6	7041 720

Table 3. Basic characteristics of the MW-size halo formed in the different DM models. We list the mass ($M_{200,\,\mathrm{crit}}$), radius ($R_{200,\,\mathrm{crit}}$), maximum circular velocity (V_{max}), radius where the maximum circular velocity is reached (R_{max}), and the number of resolved subhaloes within 300 kpc (N_{sub}).

Name	$M_{200,\,\mathrm{crit}}$ ($10^{10}\,\mathrm{M}_\odot$)	$R_{200,\,\mathrm{crit}}$ (kpc)	V_{max} ($\mathrm{km\,s^{-1}}$)	R_{max} (kpc)	N_{sub}
CDM	161.28	244.05	176.82	68.29	16 108
ETHOS-1	160.47	243.64	178.12	62.58	590
ETHOS-2	164.70	245.75	181.49	63.72	971
ETHOS-3	163.36	245.09	180.60	64.37	1080
ETHOS-4	163.76	245.30	178.78	69.18	1366

2014). It was also used to find that self-interactions can leave imprints in the stellar distribution of dwarf galaxies by performing the first SIDM simulation with baryons presented in Vogelsberger et al. (2014a).

4 RESULTS

In the following, we first discuss some features of the large-scale ($100\,h^{-1}$ Mpc) parent simulations, followed by the main focus of our work, the resimulated galactic halo. We show here only the results for CDM, and ETHOS-1 to ETHOS-3 since ETHOS-4 has the same initial power spectrum as ETHOS-3 and a significantly smaller self-interaction cross-section. The impact of SIDM effects on large scales is thus much smaller for ETHOS-4 compared to ETHOS-1 to ETHOS-3. We have therefore not performed a uniform box simulation for ETHOS-4.

4.1 Large-scale structure

We first quantify the large-scale distribution of matter in Fig. 2, where we present the dimensionless power spectra, $\Delta(k)^2 = k^3 P(k)/(2\pi^2)$, at redshifts $z = 10, 6, 4, 2, 0$ for our parent simulations. The dashed grey line shows the shot-noise power spectrum caused by the finite particle number of the simulation, it gives an indication of the resolution limit in this plot at low redshifts. The DAO features of the ETHOS-1 to ETHOS-3 models, clearly visible on the primordial power spectrum (see left-hand panel of Fig. 1), are only preserved down to $z \sim 10$ (where the first oscillation is marginally resolved for model ETHOS-1). At lower redshifts, the imprint of these features is significantly reduced and is essentially erased at $z = 0$. At this time, although the power spectra of the non-CDM simulations are relatively close to the CDM case, there is a slight suppression of power in the ETHOS-1 to ETHOS-3 models for scales smaller than $k \gtrsim 10^2\,h\,\mathrm{Mpc}^{-1}$. This suppression is largest for ETHOS-1 and smallest for ETHOS-3, which reflects the fact that the initial power spectrum damping is largest for ETHOS-1 and smallest for ETHOS-3. Our results therefore confirm the previous finding of Buckley et al. (2014), namely that in the weak DAO regime, the non-linear evolution makes the differences with CDM in the power spectra relatively small at low redshifts. We note that we do not present images of the large-scale density field since the different models are indistinguishable on these scales.

Although the power spectra are similar at $z = 0$ between the different DM models, there are significant differences in the halo mass function today due to the delay in the formation of low mass haloes at high redshift. This is shown in Fig. 3 where we plot the differential FoF mass function at $z = 0$. Here we see a clear suppression of low-mass haloes in ETHOS-1 to ETHOS-3 compared to the CDM case (below a few times $\sim 10^{11}\,\mathrm{M}_\odot$ for model ETHOS-1).

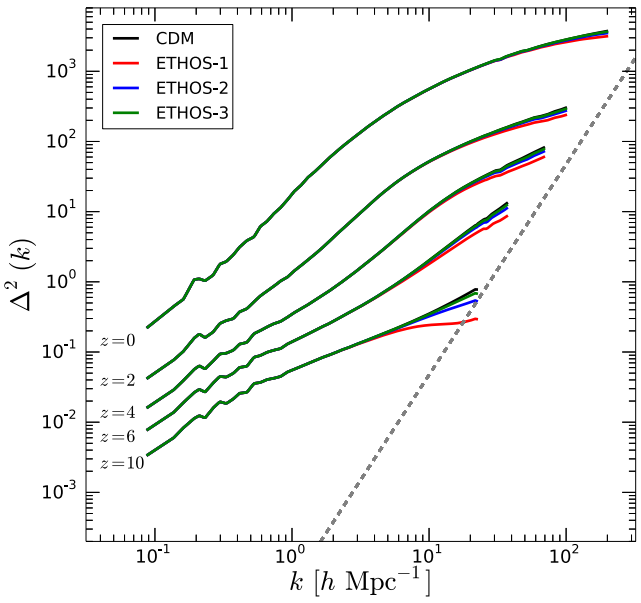

Figure 2. Non-linear dimensionless power spectra, $\Delta(k)^2 = k^3 P(k)/(2\pi^2)$, of the parent simulations for the different DM models at the indicated redshifts ($z = 10, 6, 4, 2, 0$). The dashed grey line denotes the shot-noise limit expected if the simulation particles are a Poisson sampling from a smooth underlying density field. The sampling is significantly sub-Poisson at high redshifts and in low-density regions, but approaches the Poisson limit in non-linear structures. The non-CDM models deviate significantly from CDM at high redshifts, but this difference essentially vanishes towards $z = 0$.

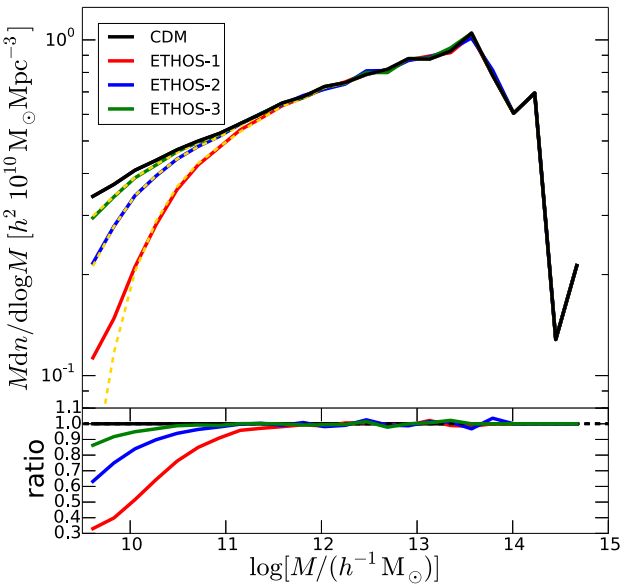

Figure 3. Differential FoF halo mass function (multiplied by FoF mass squared) for the different DM models at $z = 0$. Approximating the first DAO feature in the linear power spectrum with a sharp power-law cutoff, we show the resulting analytic estimates for the differential halo mass function of the different DM models (yellow dashed). The lower panel shows the ratios between the different simulation models relative to CDM.

The strongest suppression is seen for ETHOS-1 and the weakest for ETHOS-3. This is again expected given the initial power spectra of the different models. The lower panel of Fig. 3 shows that the suppression factor for haloes around $\sim 10^{10}\,h^{-1}\,\mathrm{M}_\odot$ is more than

a factor of 2 for ETHOS-1, whereas it is only about 10 per cent for ETHOS-3, which is therefore quite close to the CDM case at this dwarf-size scale. We show below that the suppression of the faint end of the halo mass function also carries over to the subhalo mass function. As expected, the cutoff in the initial power spectra of ETHOS-1 to ETHOS-3 reduces the halo abundance similarly as in WDM models. However, we stress again that the shape of the power spectrum cutoff in our models is different from those in typical WDM models.

We attempt to analytically understand this cutoff by modelling the first DAO feature in the linear power spectrum with a sharp power-law cutoff (see equation 6) and neglect the power contained in higher order harmonics. Following the derivation of Van den Aarssen et al. (2012), we adopt a cutoff mass $M_{\rm cut} = fM_{\rm f}$ that scales linearly with the filtering mass, $M_{\rm f}$. The scaling factor, f, accounts for differences in halo definitions (spherical overdensity versus FoF) and for differences between the simplified model of spherical collapse and our numerical cosmological simulations. We chose to adopt an exponential cutoff, $\exp(-M_{\rm cut}/M)$, to the differential CDM mass function of our particular realization so that we can exclude cosmic variance and halo suppression effects due to finite resolution. This cutoff shape appears to accurately describe the abundance of haloes seeded by primordial power rather than artificial (numerical) power due to particle discreteness effects (Wang & White 2007; Angulo, Hahn & Abel 2013).[2]

Calibrating the global scaling factor, $f \approx 2.85$, we obtain a good match to the simulated FoF mass functions and find

$$M_{\rm cut} = 10^{11} \left(\frac{m_{\rm WDM}}{\rm keV}\right)^{-4} h^{-1}\,{\rm M}_\odot. \quad (6)$$

Alternatively, we can express the cutoff as a function of the kinetic decoupling temperature $T_{\rm kd}$. In this case, we find

$$M_{\rm cut} = 5 \times 10^{10} \left(\frac{T_{\rm kd}}{100\,{\rm eV}}\right)^{-3} h^{-1}\,{\rm M}_\odot\,. \quad (7)$$

This result for the evolved, *non-linear* power spectrum agrees to within about a factor of 2 with earlier analytic estimates for this regime (Loeb & Zaldarriaga 2005; Bertschinger 2006; Bringmann 2009), based on definitions of $M_{\rm cut}$ related to the form of the *linear* power spectrum. Note that the above relation between $M_{\rm cut}$ and $T_{\rm kd}$ specifically assumes the definition of $T_{\rm kd}$ proposed in Bringmann & Hofmann (2007); other definitions of $T_{\rm kd}$ would change it by a constant factor Bringmann et al. (2016).

We also observe indications for a slight deviation from the $T_{\rm kd}^{-3}$ dependence; fully resolving this would however require to run high-resolution simulations over a much larger range of cutoff values, which is beyond the scope of this work. As a result, the effect of early DM-DR interactions on the mass function (around the cutoff region) can be approximated by an exponential cutoff due to free streaming of WDM (see yellow dashed lines in Fig. 3). However, this simple approximation ceases to be valid at masses much smaller than $M_{\rm cut}$ because SIDM models have more power in in the primordial power spectrum in comparison to WDM, which is characterized by a comparably sharp cutoff (as explicitly demonstrated by the discrepancies of the mass functions of the analytical model and the ETHOS-1 simulation). In the non-linear regime of structure formation, adjacent-modes do not evolve independently of each other and start to couple redistributing power to the valleys at the expense of the extrema. Hence, the shallower decay towards small haloes is seeded by the integrated additional power of SIDM models in comparison to WDM.

[2] We note that according to the study by Wang & White (2007), the limiting mass below which discreteness effects are important is given by $M_{\rm lim} = 10.1\,\Omega_{\rm m}\rho_{\rm crit} d k_{\rm peak}^{-2}$, where d is the interparticle separation, and $k_{\rm peak}$ is the wavenumber for which $\Delta^2_{\rm linear}$ peaks. Taking the ETHOS-1 model, which has the strongest power spectrum cutoff, we find that for our parent $100\,h^{-1}$ Mpc simulation, we have $M_{\rm lim} \sim 1.7 \times 10^9\,h^{-1}\,{\rm M}_\odot$, while for the level-3 zoom simulations (the lowest resolution level for our zoom simulations), we have $M_{\rm lim} \sim 4.2 \times 10^8\,h^{-1}\,{\rm M}_\odot$. Our simulations are thus free of spurious artefacts in the mass scales we explored.

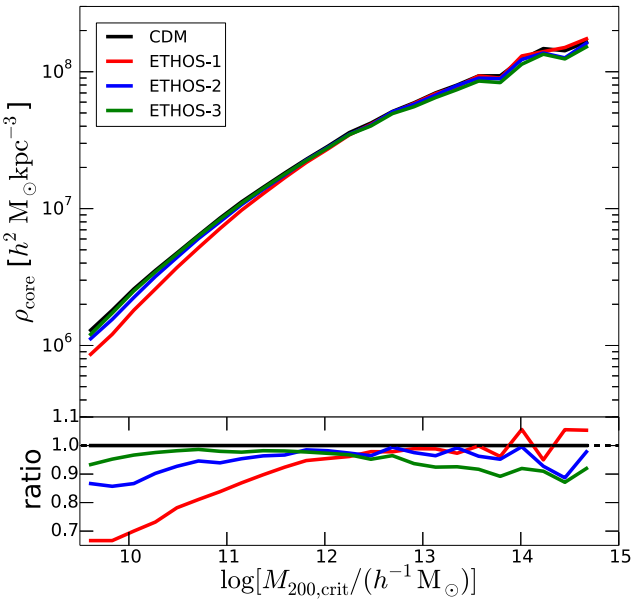

Figure 4. Central density as a function of halo mass ($M_{200,\,\rm crit}$) for all main haloes (i.e. we do not include subhaloes here) for the different DM models. The central (core) density is defined at 8.7 kpc (three times the gravitational softening length). The lower panel shows the ratio with respect to the CDM case. ETHOS-1 and ETHOS-2 show decreasing core densities towards smaller halo masses. Interestingly, ETHOS-3 shows a slightly different trend where the core density compared to CDM is most reduced for the most massive haloes in the simulation.

The effects we have discussed so far are mainly driven by the primordial damping of the DM power spectrum. They are not strongly affected by late-time DM self-interactions. As we know, self-interactions will affect the internal structure of haloes at late times, where the density is high enough to cause at least some particle collisions during a Hubble time. We can try to quantify this already at the resolution level that our parent simulation allows. To do this, we measure the central or core density for all resolved main haloes in the uniform box simulations, similar to the analysis presented in Buckley et al. (2014). The mass resolution of our uniform box is slightly better than that of Buckley et al. (2014), and we probe at the same time a volume which is about 3.8 times larger. We can therefore sample a larger range of halo masses and with better statistics. We define the central (core) density within three times the softening length (8.7 kpc). The upper panel of Fig. 4 shows the actual core density, while the lower panel shows the ratio with respect to the CDM case. We take the median value of the distribution within each mass bin. The plot shows the familiar scale of density with mass at a fixed radius, with core densities that vary from $\sim 10^6\,h^2\,{\rm M}_\odot\,{\rm kpc}^{-3}$ for halo masses around $\sim 10^{10}\,h^{-1}\,{\rm M}_\odot$ to $\sim 10^8\,h^2\,{\rm M}_\odot\,{\rm kpc}^{-3}$ for halo masses around $\sim 10^{14}\,h^{-1}\,{\rm M}_\odot$. Models ETHOS-1 (red) and ETHOS-2 (blue) have a significantly reduced core density compared to the CDM case for low-mass haloes. We

note that the effect is strongest in the former than in the latter, which points to the primordial power spectrum suppression as the main culprit since the cross-section is lower for model ETHOS-1 than for model ETHOS-2. Low-mass haloes in ETHOS-1 are therefore less dense than in CDM, mainly because they form later (analogous to the WDM case). Interestingly, ETHOS-3 shows a different behaviour. Here the core density is most reduced for massive systems. This effect is also slightly seen for ETHOS-2, but it is much more pronounced for ETHOS-3. The cause of this behaviour is DM self-scattering since ETHOS-3 has a large cross-section, even at large scales, thus, an impact on the inner structure of haloes is expected even for massive haloes (see Fig. 1). The reason we do not see a reduction in $\rho(3\epsilon)$ at low masses for the ETHOS-3 case, despite its very large cross-section at these scales, is because $3\epsilon \sim 9$ kpc is too large relative to the maximum core sizes (set by $\lesssim r_{-2}$, the radius where the logarithmic density slope is -2) that low mass haloes ($<10^{11}\,h^{-1}\,\mathrm{M}_{\odot}$) can have.

To better understand the core density behaviour we show in Fig. 5 stacked radial density profiles splitting the main haloes in different mass bins (as indicated in the legends). One can clearly see that the haloes at the low-mass end are significantly affected by both the damping of the initial power spectrum and self-interactions. The strongest density reduction occurs here for ETHOS-1, which has the largest damping scale. This is true despite model ETHOS-1 having the lowest self-interaction of all models. In other words, for the models studied here (ETHOS-1 to ETHOS-3), the suppression of the power spectrum at small scales dominates over the effect of self-interactions at low masses. This trend continues up to MW masses, where a reversal of the hierarchy of models begins to happen, with ETHOS-3 becoming the most divergent relative to CDM. Massive haloes are not strongly affected by the damping of primordial fluctuations making self-interactions the dominant mechanism. The reduction of the central density therefore responds directly to the amplitude of the cross-section.

4.2 Galactic halo

We will now focus on the analysis of the zoom-in simulation of the selected MW-sized halo. We first discuss the models ETHOS-1 to ETHOS-3 and later focus on ETHOS-4, which addresses some of the small-scale issues of CDM. Fig. 6 shows the projected DM density distribution on the scales of the MW halo for the CDM case, and for models ETHOS-1 to ETHOS-3.[3] At these scales ($\lesssim$500 kpc), the suppression of small-scale structure is clearly visible. This suppression is driven by the resolved cutoff scale in the linear power spectra of ETHOS-1 to ETHOS-3 caused by DM-DR interactions. This cutoff reduces the number of resolved subhaloes very strongly for model ETHOS-1, which has the largest damping scale. We stress once more, that self-interactions of the order discussed here mainly affect the internal structure of haloes, without significantly altering the abundance of subhaloes within MW-like haloes. Fig. 6 also demonstrates that the position and appearance of the largest subhaloes does not change significantly across the different models (except perhaps for ETHOS-1).

Due to the amplitude and velocity dependence of the cross-section for models ETHOS-1 to ETHOS-3, there is only a rather mild impact of particle collisions on the main halo properties. This can be seen in Fig. 7, where we show the density profile of the main MW halo. There is a resolved DM core with a size of $\sim$2 kpc, but it is clearly much less pronounced than the effect seen for a large constant cross-section of $\sim 10\,\mathrm{cm}^2\,\mathrm{g}^{-1}$, where the core size is $\gtrsim$50 kpc (e.g. Vogelsberger et al. 2012), this is naturally expected since at the characteristic velocities of DM particles in the MW halo, the cross-sections in our models are $<1\,\mathrm{cm}^2\,\mathrm{g}^{-1}$ (see Fig. 1). Such small cores in the MW galaxy (or Andromeda) are fully consistent with any constraints from observations (e.g. Bovy & Rix 2013). Fig. 7 also demonstrates that the core is largest for model ETHOS-3 and smallest for model ETHOS-1, which is directly explained by the relative amplitude of the cross-section in these models. We note that at the scales of the MW halo, the cutoff scale in the linear power spectrum (left-hand panel of Fig. 1) has a subdominant impact compared to the effect of DM collisions. This was already seen, albeit not as clearly, in Fig. 5.

The apparent reduction of substructure is quantified in more detail in Fig. 8, where we show the cumulative distribution of subhaloes within 300 kpc of the halo centre as a function of their peak circular velocity V_{max}. The left-hand panel shows the cumulative number on a linear scale, and includes observational data from Polisensky & Ricotti (2011). The MS problem is apparent since there are significantly more CDM subhaloes than visible satellites. This discrepancy can be solved or alleviated through a combination of photoevaporation and photoheating when the Universe was reionized, and SN feedback (e.g. Efstathiou 1992; Gnedin 2000; Benson et al. 2002; Koposov et al. 2008), although photoevaporation and photoheating alone may not be enough to bring the predicted number of massive, luminous satellites into agreement with observations (e.g. Boylan-Kolchin, Bullock & Kaplinghat 2012; Brooks et al. 2013). The plot also demonstrates that the reduction of substructure in ETHOS-1 to ETHOS-3 alleviates the abundance problem significantly. The strong damping in the power spectrum of model ETHOS-1 leads to a very significant reduction of satellites which is quite close to the data, perhaps too close given the expected impact of reionization and supernovae feedback. If these processes were to be included in our simulations with a similar strength as they are included in hydrodynamical simulations within CDM, model ETHOS-1 would be ruled out. One must be cautious however, since the strength of these processes is not known well enough, they could in fact be much weaker than currently assumed within CDM, which would lead to different conclusions. Models ETHOS-2 and ETHOS-3 show a smaller but still significant reduction of the abundance of subhaloes which spans the range between the CDM result and the observed satellite population. The right-hand panel of Fig. 8 shows the same quantity on a logarithmic scale. We note that our main objective here is to show that in the ETHOS models we explored, there is a substantial effect on the number of satellites (due to the power spectrum cutoff) and in the inner halo densities (a combination of the power spectrum cutoff and the self-interaction cross-section). A more definitive solution to the MS problem within ETHOS would require the inclusion of the baryonic processes mentioned above. It is interesting to note that the reduction to the subhalo abundance in ETHOS-3 is approximately a factor of 2 at 20 km s^{-1}, which is only slightly smaller than the reduction achieved by current hydrodynamical simulations that include baryonic physics (see fig. 4 of Sawala et al. 2016).

Finally, we show the (radially averaged) internal structure of subhaloes in Fig. 9. Here we select for each model the 15 subhaloes with the largest present-day V_{max} values and plot the distribution of density profiles (left-hand panel) and circular velocity profiles (right-hand panel). The thick lines show the median of the distribution, whereas the shaded region shows the lower and upper envelopes.

[3] High-resolution images and movies can be found at http://mvogelsb.scripts.mit.edu/ethos.php

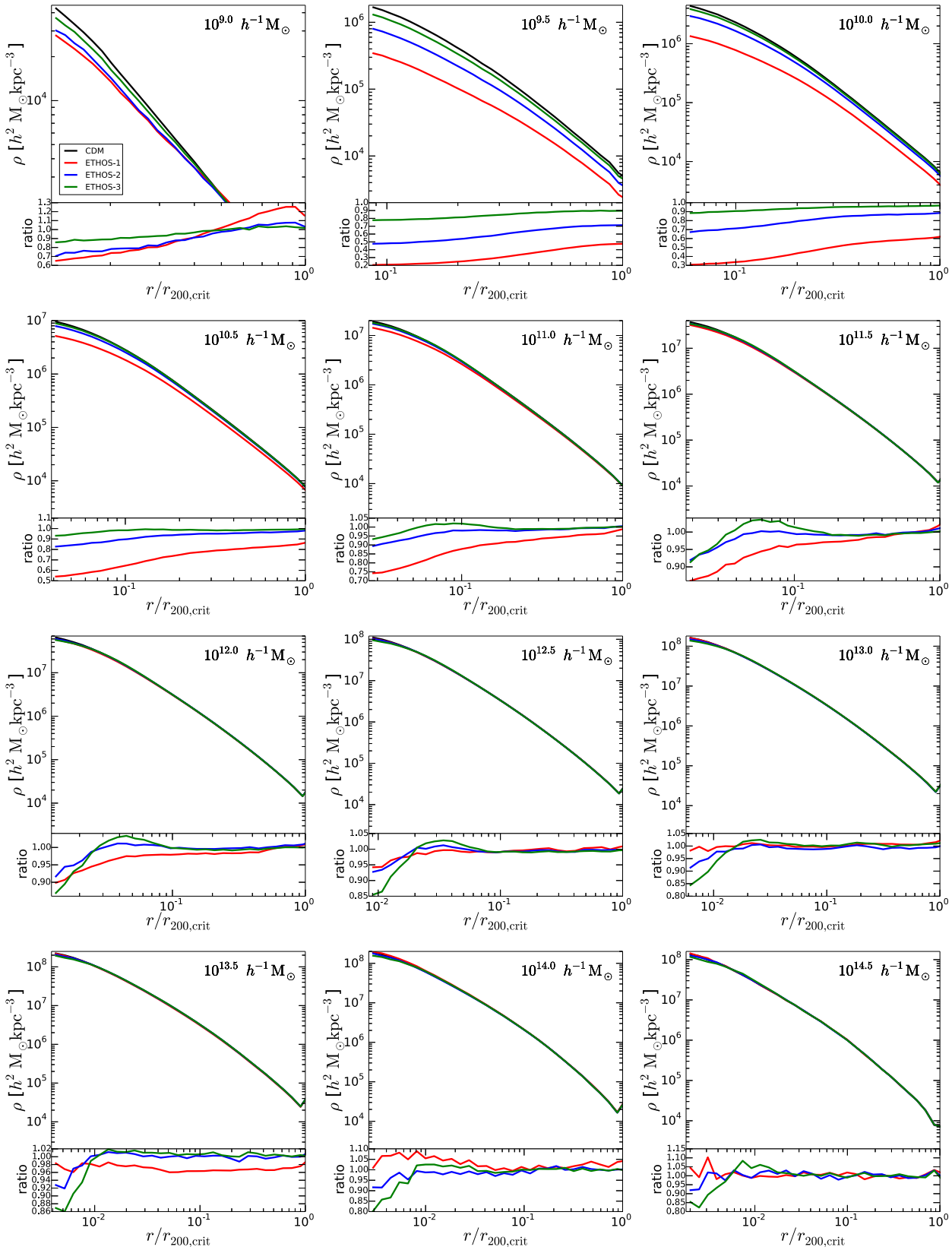

Figure 5. Stacked density profiles for different halo mass ranges ($M_{200,\,\mathrm{crit}}$) as indicated in each panel for our different DM models. We show the profiles starting at 2 kpc out to the virial radius. One can clearly see that the different non-CDM models affect the profiles in rather different ways depending on the mass scale.

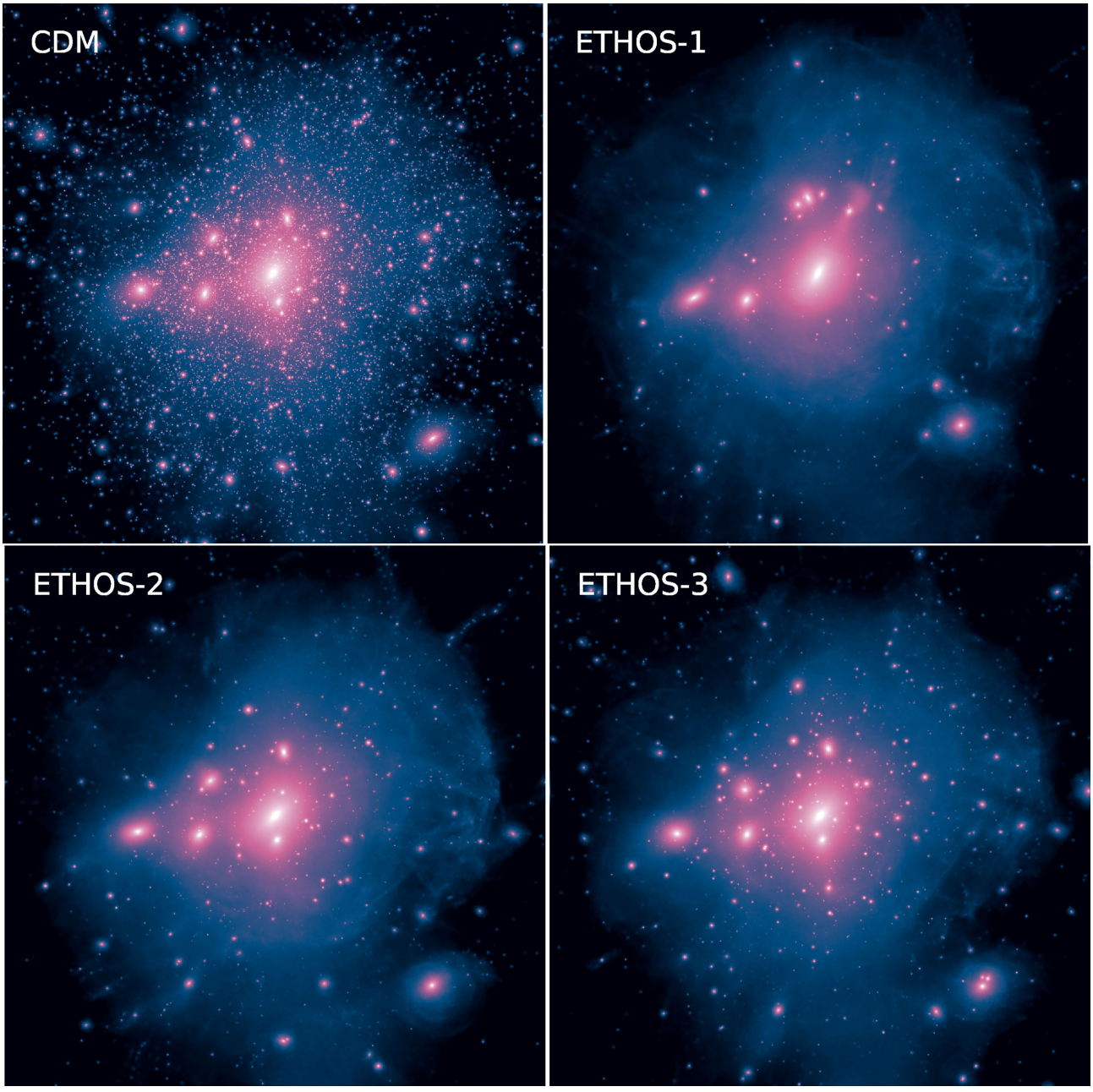

Figure 6. DM density projections of the zoom MW-like halo simulations for four different DM models. The suppression of substructure, relative to the CDM model, is evident for the ETHOS models ETHOS-1 to ETHOS-3, which have a primordial power spectrum suppressed at small scales. The projection has a side length and depth of 500 kpc.

We only consider subhaloes that are within 300 kpc halocentric distance. The right-hand panel also contains observational data from nine of the classical MW dSphs taken from Wolf et al. (2010). The distribution of circular velocities for the CDM model clearly shows the well-known TBTF problem, while the density profiles points to the also well-known CC problem: if Fornax is cored for instance, the size of its DM core is between 0.6 and 1.8 kpc (Amorisco, Agnello & Evans 2013), which cannot be accommodated in the CDM model. The non-CDM models on the other hand show clearly reduced (density) circular velocity profiles, which are seemingly too low compared to what is required by the data. We show below that the combination of self-interactions and the damping in the initial power spectrum is responsible for this strong reduction. This is quite different from the results shown in Vogelsberger et al. (2012), where we only considered the effect of self-interactions. The fact that models ETHOS-1 to ETHOS-3 do not fit the data is unsurprising since those models were not specifically tuned to reproduce the subhalo statistics of the MW. They were rather picked out of a large particle physics parameter space. This result however shows that it can actually be quite difficult to predict a priori the combined impact of self-scattering and primordial damping on the highly non-linear evolution that leads to the internal structure of subhaloes. It also shows the potential of the MW satellites data to constrain the parameter space of our effective framework.

We should note that the severity of the TBTF problem in the MW depends on the MW halo mass. For low halo masses $\lesssim 8 \times 10^{11} \mathrm{M}_{\odot}$,

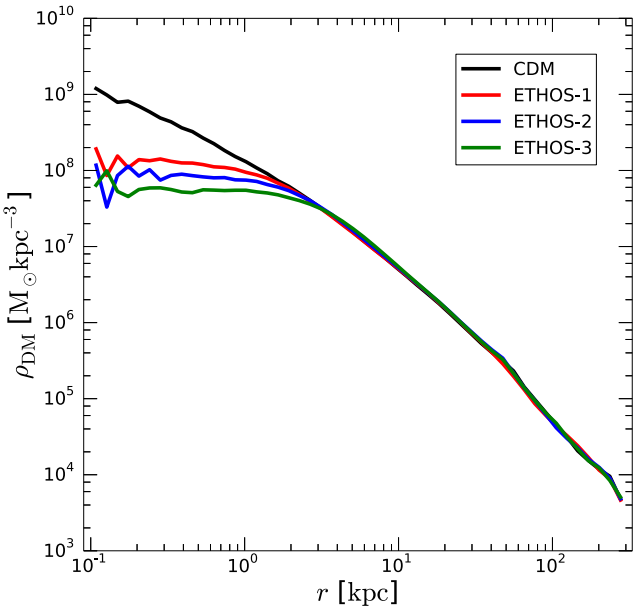

Figure 7. Spherically averaged density profiles of the MW-size haloes for the four different DM models. The non-CDM models have only a mild impact on the central density profile where self-interactions lead to the formation of a small core (∼2 kpc), with a size that correlates with the amplitude of the scattering cross-section. The damping in the initial power spectrum for these models (see left-hand panel of Fig. 1) has only a secondary impact on the density profiles of MW-size haloes.

the problem disappears (e.g. Wang et al. 2012). Since we are using a halo with a mass of 1.6×10^{12} M$_\odot$, the TBTF is quite clear in our CDM simulation. This dependence on the halo mass has been discussed elsewhere. For the purpose of our work, we show a case where the problem is clear, and focus on studying the DM models that can alleviate it.

4.3 Disentangling the impact of late DM self-interactions versus early DM-DR interactions

In this section, we try to disentangle the impact of the damping of the initial power spectrum and the late-time effect of DM self-interactions. To this end we reran the MW halo for models ETHOS-1 to ETHOS-3, at resolution level-2, which has converged reasonably in the inner structure of the most massive subhaloes as can be seen in Fig. 10, where we compare level-1 (dashed) and level-2 (solid). For these resimulations we either only consider a modification to the power spectrum or only self-interactions. We can then contrast these two variations of each model with its full version and see which new DM physics is responsible for which effect. These different variations are summarized in Table 4, and are labelled ETHOS-X-sidm and ETHOS-X-power, where $X = 1, 2, 3$.

For the ETHOS-X-sidm models, we only consider self-interactions and use the same transfer function as for the CDM simulation. The ETHOS-X-power simulations, on the other hand, do not include self-interactions, but use the corresponding damped initial power spectra. We are specifically interested in the abundance and the internal structure of the subhalo population at $z = 0$. In Fig. 10, we show the subhalo mass function as a function of $V_{\rm max}$ (left-hand panel) and the circular velocity profile for the top 15 subhaloes (right-hand panel) for the different reduced models (each in a row as shown in the legends). The most striking impact can be seen when looking at the ETHOS-X-sidm results, which do not include the damping of the initial power spectrum at small scales. Self-interactions do not affect the abundance of subhaloes, at least at the amplitude of the cross-sections we consider here (see also Vogelsberger et al. 2012). The values of $V_{\rm max}$ are also not affected significantly compared to CDM, it is only within $r_{\rm max}$ where the

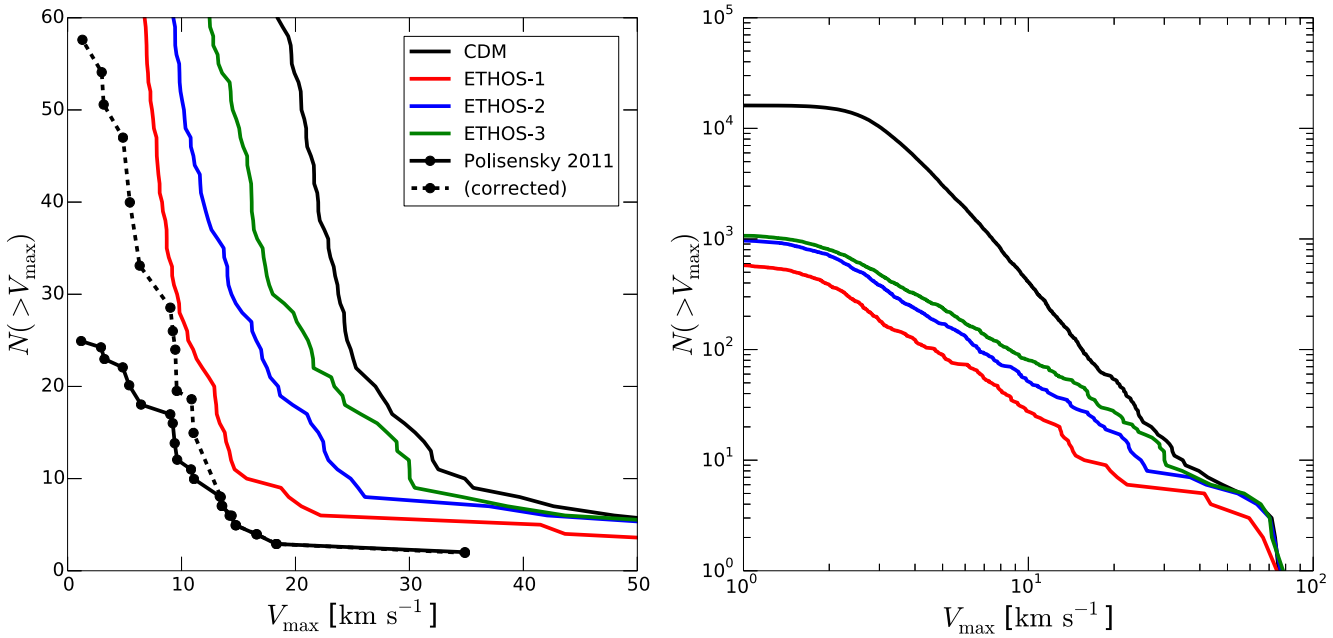

Figure 8. The number of subhaloes as a function of their maximal circular velocity for the four different DM models. We include all subhaloes with a halocentric distance less than 300 kpc. Left-hand panel: linear scale with a comparison to observed satellites of the MW including a sky coverage correction (Polisensky & Ricotti 2011). The discrepancy between the number of observed satellites and resolved DM subhaloes is significantly reduced in the models ETHOS-1 to ETHOS-3. Right-hand panel: log–log scale. The plateau at low $V_{\rm max}$ values is caused by limited resolution.

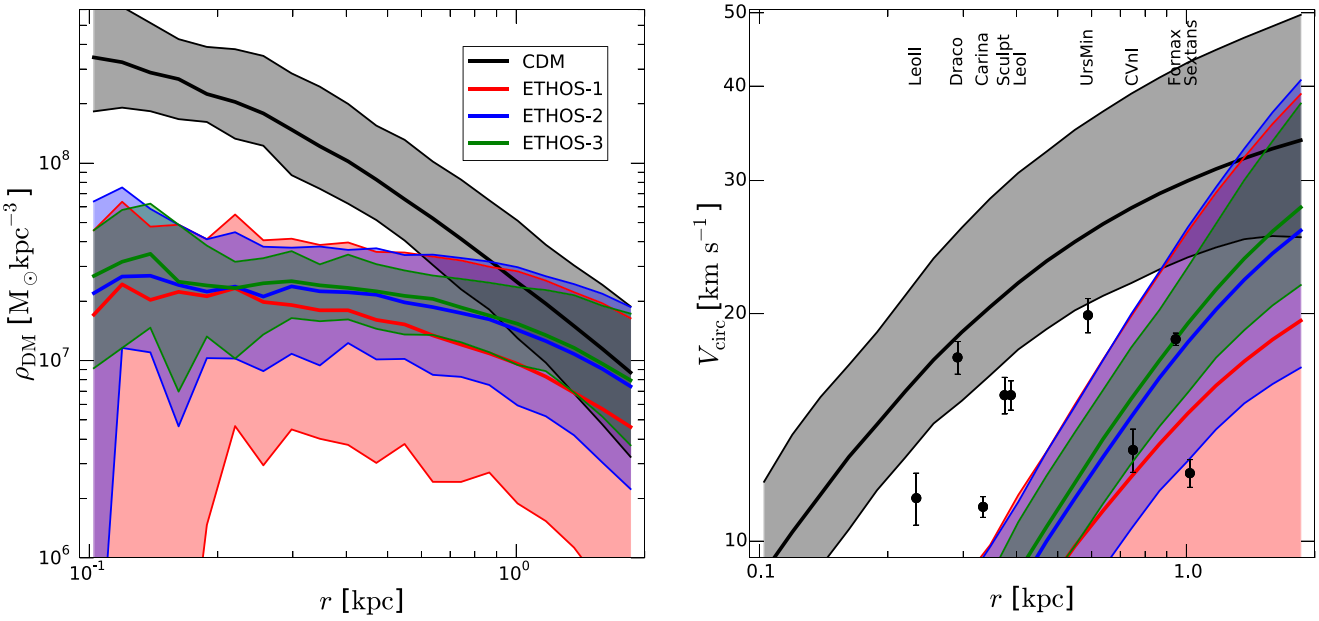

Figure 9. Internal subhalo structure for different DM models. Left-hand panel: density profile of the 15 subhaloes with the largest $V_{\rm max}$ within 300 kpc. The CDM subhaloes have cuspy density profiles, while the subhaloes in models ETHOS-1 to ETHOS-3 develop an $\gtrsim$2 kpc core. Right-hand panel: circular velocity profiles of the same subhaloes. The data points on the right are for the classical MW dSphs taken from Wolf et al. (2010). The CDM model shows the TBTF problem; i.e. the most massive subhaloes in the simulation are too dense to host most of the classical MW dSphs. The combination of damping in the initial power spectrum and self-interactions lead to a very drastic reduction of inner densities and circular velocities (enclosed mass), which seem to be inconsistent with the data.

effect of DM collisions is clear. The larger the cross-section, the stronger the reduction of the enclosed mass within $r_{\rm max}$. We note that the dispersion in the distribution of the subhalo densities is quite small in these reduced ETHOS-X-sidm models. This is because the maximum central core density cannot be lower than the density at $r_{\rm max}$, thus subhaloes with a similar $V_{\rm max}$ and $r_{\rm max}$ will develop a similar core density. Modifying the initial power spectrum naturally reduces the subhalo abundance and creates a broad dispersion in the distribution of velocity curves of the most massive subhaloes. This distribution is shifted down towards lower densities. These properties are ultimately connected to the (mass-dependent) delay in the formation of haloes caused by the primordial damping to the power spectrum. Therefore a cutoff in the primordial power spectrum creates a dispersion in the circular velocity profiles of haloes with sizes around the cutoff scale. This might help to alleviate the problem of diversity of rotation curves present in dwarf galaxies as pointed by Oman et al. (2015), albeit this problem was shown clearly only at larger scales ($V_{\rm max} \sim 100\,{\rm km\ s^{-1}}$) than the ones studied here. Current hydrodynamical simulations fail to reproduce this diversity in the inner regions of dwarf galaxies; i.e. there exists currently no viable solution for this problem within CDM even if baryonic processes are considered (Oman et al. 2015).

From the right-hand panel of Fig. 10, we can conclude that the central subhalo densities in the full model ETHOS-1 are mainly due to the damping of primordial perturbations caused by early DM-DR interactions, while for model ETHOS-3, they are essentially given by the large amplitude of the DM–DM collisions. Model ETHOS-2 lies somewhere in between.

4.4 A tuned DM model

So far we have seen that the models ETHOS-1 to ETHOS-3 affect the subhalo population of galactic haloes in different and significant ways. However, none of these models seem to provide a good fit to the actual satellite population of the MW. Most importantly, these models 'oversolve' the TBTF problem, and likely the CC problem as well, due to the combined effect of a strong damping of the initial linear power spectrum and a rather large cross-section at the characteristic velocities within the satellites. We therefore search in the parameter space of ETHOS for a model that can alleviate the abundance and structural problems of CDM simultaneously. It turns out that it is actually difficult to find a combination of damping scale and self-interaction cross-section that alleviates both of these problems. This difficulty implies that by trying to solve the MW CDM problems, we need to significantly reduce the parameter space of ETHOS. If we assume that the solution to these problems is largely driven by the particle nature of DM, we can therefore use this 'tuning process' to indirectly constrain our underlying DM particle physics models. This approach is similar to that of Bœhm et al. (2014).

We have used the results of models ETHOS-1 to ETHOS-3 to find a new model (ETHOS-4) which gives a reasonable fit to the observational data of the MW satellite population. This means that we had to iterate over different simulations (at resolution level-2) with different cutoff scale to the power spectrum and different cross-sections, using models ETHOS-1 to ETHOS-3 as references. Clearly, the cutoff of this new model needed to be on smaller scales than that of ETHOS-1 and ETHOS-2 since both models predict a very strong impact on subhalo densities, too strong to be consistent with the kinematics of MW dSphs. Furthermore, the cross-section of the self-interactions at the dwarf velocity scale should be smaller than that of ETHOS-1 to ETHOS-3 since these models (even their reduced ETHOS-X-sidm versions) oversolve the TBTF problem. Based on these considerations we have found model ETHOS-4, as a suitable candidate (see Table 1 for the parameters of this model). The initial power spectra of ETHOS-3 and ETHOS-4 are essentially

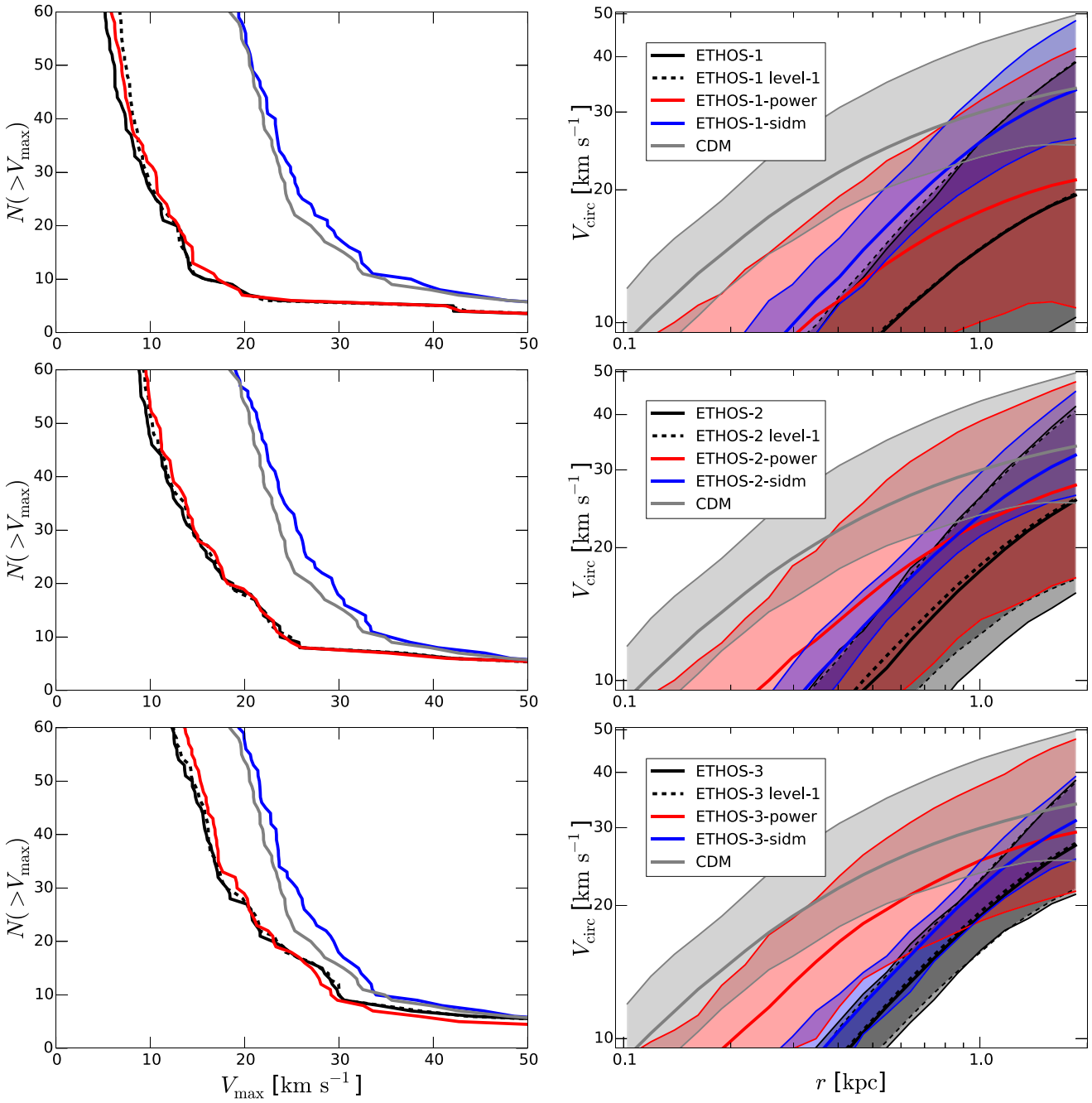

Figure 10. Properties of the subhalo population at $z = 0$ in the reduced DM models summarized in Table 4. Left-hand panel: subhalo abundance shown as a cumulative $V_{\rm max}$ plot. Right-hand panel: internal subhalo structure revealed by the circular velocity curves. We show from top to bottom the different models ETHOS-1 to ETHOS-3 along with their reduced versions. These reduced versions consider only DM self-interactions (ETHOS-X-sidm) or only a damping in the initial power spectrum due to DM-DR interactions (ETHOS-X-power). The latter affects both the abundance of subhaloes and the normalization of the circular velocity curves. Self-interactions only reduce the inner circular velocities (enclosed masses), but do not alter the abundance.

the same as can be seen in Fig. 1 (left-hand panel). This results in a very similar suppression of the number of satellites, which can clearly be seen in the left-hand panel of Fig. 11. The cross-section, on the other hand, is radically different and for low velocities more than an order of magnitude smaller than ETHOS-1. This is the key feature of model ETHOS-4: the lower cross-section results in an increased central density and larger circular velocities compared to the ETHOS-1 to ETHOS-3 models. This can clearly be seen in the right-hand panel of Fig. 11. Model ETHOS-4 demonstrates that we can find parameters for our particle physics model, and thus ETHOS parameters. Other particle physics models that map into similar parameters to ETHOS-4 should give similar results. that can alleviate the main CDM tensions at small scales. We note that this model also satisfies all current large-scale constraints as well since it deviates even less from CDM than the models ETHOS-1 to ETHOS-3. A density map of the DM distribution in this model ETHOS-4 is shown in Fig. 12. There are only little differences with respect to ETHOS-3, which are due to the significantly smaller cross-section

Table 4. Overview of reduced DM models. These models are similar to ETHOS-1 to ETHOS-3, but they only include self-interactions without the damping of the power spectrum ('sidm'), or they do not include self-interactions, but have the damping of the primordial power spectrum ('power'). The reduced models help us to disentangle these two effects present in our full models.

Name	Reduced model
ETHOS-1-sidm	ETHOS-1, only self-int. w/CDM transfer fct.
ETHOS-1-power	ETHOS-1, no self-int.
ETHOS-2-sidm	ETHOS-2, only self-int. w/CDM transfer fct.
ETHOS-2-power	ETHOS-2, no self-int.
ETHOS-3-sidm	ETHOS-3, only self-int. w/CDM transfer fct.
ETHOS-3-power	ETHOS-3, no self-int.

of ETHOS-4 compared to ETHOS-3. We note that despite having considerably lower cross-sections than the other models we explored, self-interactions are still relevant in ETHOS-4. We have verified that the central densities in subhaloes are lower (albeit the effect is relatively small) in ETHOS-4 than in a setting with the same features but with the self-interactions turned off.

We note that ETHOS-4 alleviates the tension between theory and observations for the TBTF and MS problems, but our MW-size simulations cannot be used to study directly if such a model could also produce the large cores seemingly inferred in low surface brightness galaxies (e.g. Kuzio de Naray, McGaugh & de Blok 2008), which might require large cross-sections in an interpretation based on DM collisions (see fig. 1 of Kaplinghat et al. 2016). However, besides pure DM self-interactions, ETHOS-4 also includes a relevant effect due to the damping of the power spectrum. Both effects could combine to reduce densities sufficiently to be consistent with observation of LSB galaxies. Furthermore, the character of this interplay could

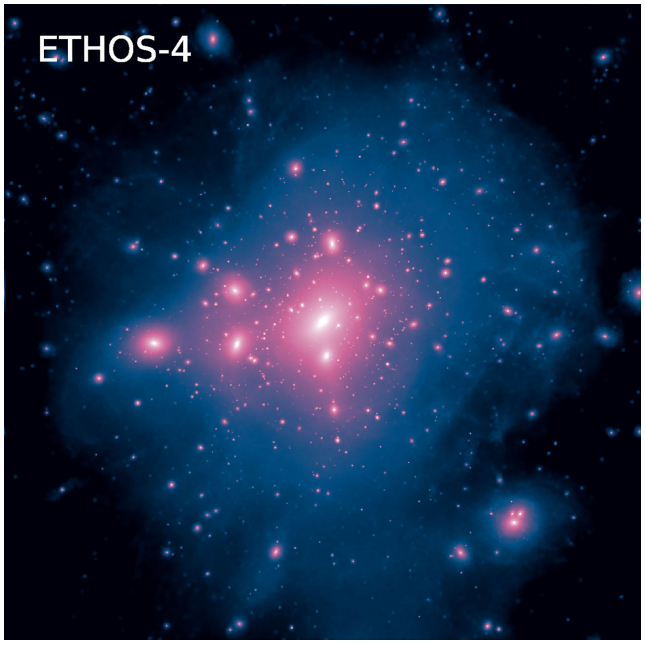

Figure 12. DM density projections of the zoom MW-like halo simulations for the tuned model ETHOS-4. The projection has a side length and depth of 500 kpc. The initial power spectrum is essentially the same as in ETHOS-3. The amount of substructure and the general DM density distribution looks very similar to ETHOS-3. Remaining differences are driven by the very different self-scattering cross-section between ETHOS-3 and ETHOS-4.

be adjusted relative to ETHOS-4 parameters by increasing the normalization of the cross-section and increasing slightly the scale for the power spectrum cut off. This would enhance the SIDM-driven core creation, while retaining significant deviations from CDM in

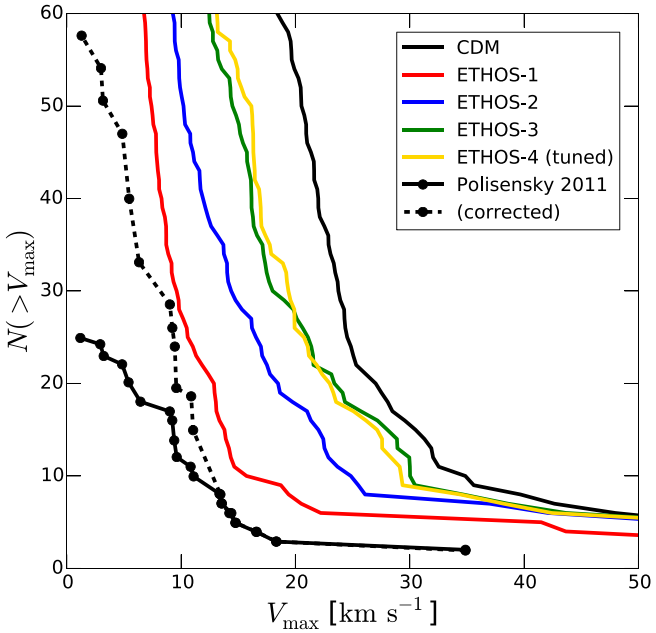

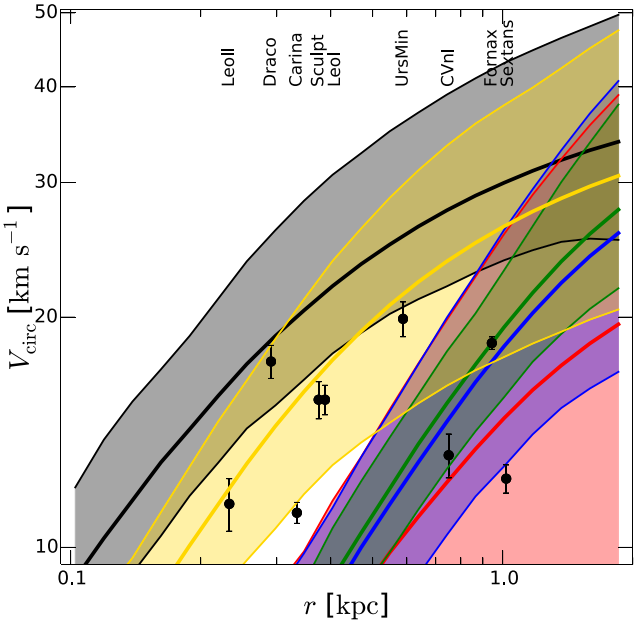

Figure 11. Subhalo population for the tuned model ETHOS-4. This model was specifically set up to address the MS and TBTF problems. Left-hand panel: the number of satellite galaxies as a function of their maximal circular velocity for the four different models with a comparison to observed satellites of the MW including a sky coverage correction (Polisensky & Ricotti 2011). We show all subhaloes with a halocentric distance less than 300 kpc. Right-hand panel: circular velocity profiles of the same haloes. The data points show MW dSphs taken from Wolf et al. (2010). The ETHOS-4 model provides a reasonable fit to the subhalo population of the MW.

the abundance of dwarf systems. We plan to explore these issues in more detail in upcoming works.

5 CONCLUSION

We have explored simulations of SIDM, which come from a particle physics model with a single DM particle interacting with itself and with a massless neutrino-like fermion (DR) via a massive mediator. The parameters of the particle physics model are mapped into an effective framework of structure formation (ETHOS, see Cyr-Racine et al. 2015), where each model is described by a specific initial power spectrum and a velocity-dependent self-interaction cross-section.

In this paper, we have analysed a few benchmark cases in the large parameter space of ETHOS, which mainly have relevant consequences for the formation and evolution of dwarf-scale haloes. We have simulated these cases in $(100\,h^{-1}\,\mathrm{Mpc})^3$ uniform boxes with 1024^3 DM particles. A galactic MW-size halo was then selected from this box and simulated at higher resolution. Our main focus is the study of this galactic halo and its subhalo population. Our highest resolution simulation has a Plummer-equivalent softening length of 72.4 pc, and a mass resolution of $2.8 \times 10^4\,\mathrm{M}_\odot$. We simulate this halo in five different models: CDM and four SIDM models (ETHOS-1 to ETHOS-4). Our main conclusion is that such models cannot only change the internal structure of subhaloes, but also affect the subhalo abundance in a similar way to WDM models, due to the inherit damping in the initial power spectrum. However, unlike WDM models, the damping in our effective models is much richer since it also contains oscillatory features caused by interaction between DM and DR in the early Universe.

Our main findings are as follows.

(i) The large-scale structure is unaffected in all our non-CDM models. At $z = 0$, the matter power spectra of the different models agree with that of CDM for $k \lesssim 200\,h^{-1}\,\mathrm{Mpc}$ (Fig. 2). The halo mass functions also agree above $\sim 10^{11}\,h^{-1}\,\mathrm{M}_\odot$, but there is a clear departure from CDM below this scale, which is mostly driven by the primordial damping in the power spectrum (see Fig. 3). We complement our simulations by analytical insight and provide a mapping from the primordial damping scale in the power spectrum to the cutoff scale in the halo mass function and the kinetic decoupling temperature.

(ii) The inner (core) density (within a fixed physical radius of 8.7 kpc) is reduced mostly in the low-mass haloes since the impact of self-interactions and power spectrum damping is the largest at those masses in the models we explored. Inner densities are affected below $10^{12}\,h^{-1}\,\mathrm{M}_\odot$ and can be reduced by up to 30 per cent for haloes around $10^{10}\,h^{-1}\,\mathrm{M}_\odot$, relative to CDM (Fig. 5). In the model with the largest cross-section (ETHOS-3), we also find a mild reduction of the central density in cluster scale haloes.

(iii) The density profile of MW-size haloes shows a small core $\lesssim$2 kpc in the SIDM models, with the core size being the largest for the model with the largest scattering cross-section (Fig. 7).

(iv) The subhalo abundance is strongly affected by the damping of the initial linear power spectrum. The selected models span the whole range between the CDM prediction and the observed satellite population (completeness corrected) of the MW (Fig. 8). One of our models, ETHOS-1, would most likely be ruled out by observational data if baryonic processes were to be included, i.e. supernovae feedback, early heating by reionization and tidal stripping.

(v) The internal structure of subhaloes is affected by both self-interactions and the primordial damping of the power spectrum reducing the enclosed mass in the inner regions and producing central density cores for the most massive subhaloes. Three of our benchmark cases (ETHOS-1 to ETHOS-3) 'oversolve' the TBTF problem in the sense that they reduce the central mass of subhaloes too strongly. The resulting circular velocity curves then lie below the observational data points coming from the inferred kinematics of the classical MW dSphs (Fig. 9). This implies that ETHOS models can actually be constrained by comparing to observational data. The large impact on the structure and appearance of massive subhaloes can also be seen in Fig. 13, where we show density maps of the two most massive subhaloes for the CDM and ETHOS-4 model.

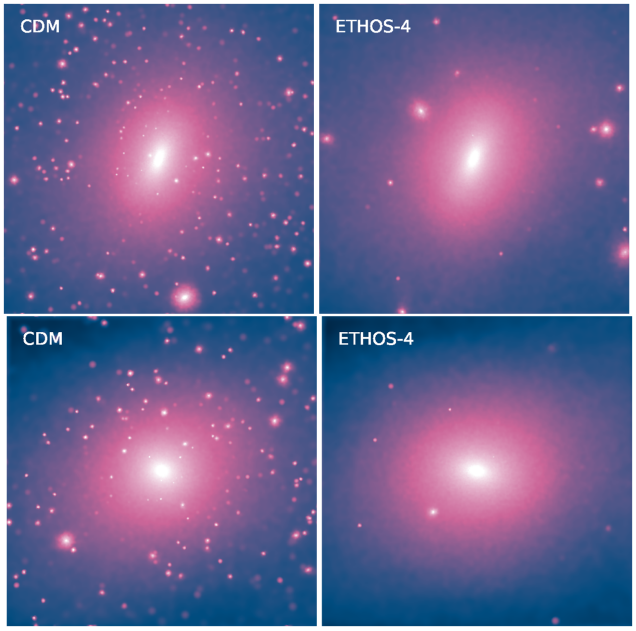

Figure 13. DM density projections of the two most massive subhaloes (within 300 kpc halocentric distance) in the MW-like halo simulations for CDM and the tuned model ETHOS-4. The projection has a side length and depth of 50 kpc.

(vi) We have searched over the parameter space of ETHOS to construct one model (ETHOS-4), which solves the TBTF problem and at the same time alleviates the MS problem (Fig. 11).

(vii) We also notice that introducing a cutoff in the primordial power spectrum (in our case caused by DM-DR interactions), is a natural way to create a dispersion in the circular velocity profiles of haloes with sizes around the cutoff scale. This might help to alleviate the problem of diversity of rotation curves present in dwarf galaxies (Oman et al. 2015); albeit this problem has only been reported at scales larger than the ones discussed here. We stress that current hydrodynamical simulations fail to reproduce this diversity in the inner regions of dwarf galaxies; i.e. there exists currently no viable solution for this problem within CDM even if baryonic processes are considered.

We have demonstrated that despite the larger accessible parameter space of our particle physics models, it is by no means trivial to find a viable and promising DM solution to some of the small-scale problems of galaxy formation. Instead, we found a surprising non-linear amplification of the effects of late DM self-interactions and early DM-DR interactions on the inner velocity profiles, which complicates any simple inference of the underlying particle physics nature from astrophysical constraints. We conclude that the effective models discussed here provide an interesting alternative to CDM

by being capable of solving some of its outstanding small-scale problems by exploring a richer (but allowed) DM phenomenology. Specifically, those models might be able to solve or alleviate the TBTF problem, the MS problem, the CC problem and produce a larger diversity of dwarf galaxy rotation curves simultaneously.

The parameter space of this generalization of the structure formation theory can be constrained by contrasting model predictions to observations, particularly when baryonic processes are added into the theory. Albeit the increased parameter space makes this effective framework more complex than CDM, it is a complexity that is necessary given our incomplete knowledge of both the DM nature and the strength of the key baryonic processes affecting galaxy formation and evolution. Clearly, our effective theory needs to be explored in much more detail including its interplay with baryonic physics. We will address these questions in the future.

ACKNOWLEDGEMENTS

We thank Michael Boylan-Kolchin, Federico Marinacci for useful comments, and Volker Springel for giving us access to AREPO. The simulations were performed on the joint MIT-Harvard computing cluster supported by MKI and FAS. MV acknowledges support through an MIT RSC award. The Dark Cosmology Centre is funded by the DNRF. JZ is supported by the EU under a Marie Curie International Incoming Fellowship, contract PIIF-GA-2013-62772. KS gratefully acknowledges support from the Friends of the Institute for Advanced Study. The research of KS is supported in part by a National Science and Engineering Research Council (NSERC) of Canada Discovery Grant. F-Y C-R acknowledges the support of the National Aeronautical and Space Administration ATP grant 14-ATP14- 0018 at Harvard University. The work of F-Y C-R was performed in part at the California Institute of Technology for the Keck Institute for Space Studies, which is funded by the W. M. Keck Foundation. CP gratefully acknowledges the support of the Klaus Tschira Foundation.

REFERENCES

Ackerman L., Buckley M. R., Carroll S. M., Kamionkowski M., 2009, Phys. Rev. D, 79, 023519
Amorisco N. C., Agnello A., Evans N. W., 2013, MNRAS, 429, L89
Angulo R. E., Hahn O., Abel T., 2013, MNRAS, 434, 3337
Benson A. J., Frenk C. S., Lacey C. G., Baugh C. M., Cole S., 2002, MNRAS, 333, 177
Bertone G., 2010, Nature, 468, 389
Bertone G., Hooper D., Silk J., 2005, Phys. Rep., 405, 279
Bertschinger E., 2006, Phys. Rev. D, 74, 063509
Blumenthal G. R., Faber S. M., Primack J. R., Rees M. J., 1984, Nature, 311, 517
Bode P., Ostriker J. P., Turok N., 2001, ApJ, 556, 93
Borzumati F., Bringmann T., Ullio P., 2008, Phys. Rev. D, 77, 063514
Bovy J., Rix H.-W., 2013, ApJ, 779, 115
Boyarsky A., Lesgourgues J., Ruchayskiy O., Viel M., 2009, Phys. Rev. Lett., 102, 201304
Boylan-Kolchin M., Bullock J. S., Kaplinghat M., 2011, MNRAS, 415, L40
Boylan-Kolchin M., Bullock J. S., Kaplinghat M., 2012, MNRAS, 422, 1203
Bringmann T., 2009, New J. Phys., 11, 105027
Bringmann T., Hofmann S., 2007, J. Cosmol. Astropart. Phys., 4, 016
Bringmann T., Hasenkamp J., Kersten J., 2014, J. Cosmol. Astropart. Phys., 7, 42
Bringmann T., Tveit Ihle H., Kersten J., Walia P., 2016, preprint (arXiv:1603.04884)
Brook C. B., 2015, MNRAS, 454, 1719
Brook C. B., Di Cintio A., 2015, MNRAS, 450, 3920
Brook C. B., Shankar F., 2016, MNRAS, 455, 3841
Brooks A., 2014, Ann. Phys., Lpz., 526, 294
Brooks A. M., Kuhlen M., Zolotov A., Hooper D., 2013, ApJ, 765, 22
Buckley M. R., Fox P. J., 2010, Phys. Rev. D, 81, 083522
Buckley M. R., Zavala J., Cyr-Racine F.-Y., Sigurdson K., Vogelsberger M., 2014, Phys. Rev. D, 90, 043524
Bœhm C., Riazuelo A., Hansen S. H., Schaeffer R., 2002, Phys. Rev. D, 66, 083505
Bœhm C., Schewtschenko J. A., Wilkinson R. J., Baugh C. M., Pascoli S., 2014, MNRAS, 445, L31
Cautun M., Bose S., Frenk C. S., Guo Q., Han J., Hellwing W. A., Sawala T., Wang W., 2015, MNRAS, 452, 3838
Chan T. K., Kereš D., Oñorbe J., Hopkins P. F., Muratov A. L., Faucher-Giguère C.-A., Quataert E., 2015, MNRAS, 454, 2981
Cyr-Racine F.-Y., Sigurdson K., 2013, Phys. Rev. D, 87, 103515
Cyr-Racine F.-Y., Sigurdson K., Zavala J., Bringmann T., Vogelsberger M., Pfrommer C., 2015, preprint (arXiv:1512.05344)
Dasgupta B., Kopp J., 2014, Phys. Rev. Lett., 112, 031803
Davis M., Efstathiou G., Frenk C. S., White S. D. M., 1985, ApJ, 292, 371
De Blok W. J. G., McGaugh S. S., 1997, MNRAS, 290, 533
Efstathiou G., 1992, MNRAS, 256, 43
Feng J. L., Kaplinghat M., Tu H., Yu H.-B., 2009, J. Cosmol. Astropart. Phys., 7, 4
Feng J. L., Kaplinghat M., Yu H.-B., 2010, Phys. Rev. Lett., 104, 151301
Garzilli A., Boyarsky A., Ruchayskiy O., 2015, preprint (arXiv:1510.07006)
Gillet N., Ocvirk P., Aubert D., Knebe A., Libeskind N., Yepes G., Gottlöber S., Hoffman Y., 2015, ApJ, 800, 34
Gnedin N. Y., 2000, ApJ, 542, 535
Hahn O., Abel T., 2011, MNRAS, 415, 2101
Hu W., Barkana R., Gruzinov A., 2000, Phys. Rev. Lett., 85, 1158
Jungman G., Kamionkowski M., Griest K., 1996, Phys. Rep., 267, 195
Kahlhoefer F., Schmidt-Hoberg K., Frandsen M. T., Sarkar S., 2014, MNRAS, 437, 2865
Kahlhoefer F., Schmidt-Hoberg K., Kummer J., Sarkar S., 2015, MNRAS, 452, L54
Kamada A., Yoshida N., Kohri K., Takahashi T., 2013, J. Cosmol. Astropart. Phys., 3, 008
Kaplinghat M., 2005, Phys. Rev. D, 72, 063510
Kaplinghat M., Keeley R. E., Linden T., Yu H.-B., 2014, Phys. Rev. Lett., 113, 021302
Kaplinghat M., Tulin S., Yu H.-B., 2016, Phys. Rev. Lett., 116, 041302
Kauffmann G., 2014, MNRAS, 441, 2717
Klypin A., Kravtsov A. V., Valenzuela O., Prada F., 1999, ApJ, 522, 82
Klypin A., Karachentsev I., Makarov D., Nasonova O., 2015, MNRAS, 454, 1798
Koposov S. et al., 2008, ApJ, 686, 279
Kuzio de Naray R., McGaugh S. S., de Blok W. J. G., 2008, ApJ, 676, 920
Kuzio de Naray R., Martinez G. D., Bullock J. S., Kaplinghat M., 2010, ApJ, 710, L161
Lewis A., Challinor A., 2011, Astrophysics Source Code Library, record ascl:1102.026
Loeb A., Weiner N., 2011, Phys. Rev. Lett., 106, 171302
Loeb A., Zaldarriaga M., 2005, Phys. Rev. D, 71, 103520
Lovell M. R. et al., 2012, MNRAS, 420, 2318
Macciò A. V., Paduroiu S., Anderhalden D., Schneider A., Moore B., 2012, MNRAS, 424, 1105
Massey R. et al., 2015, MNRAS, 449, 3393
Medvedev M. V., 2014, Phys. Rev. Lett., 113, 071303
Moore B., Ghigna S., Governato F., Lake G., Quinn T., Stadel J., Tozzi P., 1999, ApJ, 524, L19
Navarro J. F., Eke V. R., Frenk C. S., 1996, MNRAS, 283, L72
Oh S.-H., de Blok W. J. G., Brinks E., Walter F., Kennicutt R. C., Jr, 2011, AJ, 141, 193
Oman K. A. et al., 2015, MNRAS, 452, 3650
Papastergis E., Martin A. M., Giovanelli R., Haynes M. P., 2011, ApJ, 739, 38
Papastergis E., Giovanelli R., Haynes M. P., Shankar F., 2015, A&A, 574, A113

Pawlowski M. S., Kroupa P., Jerjen H., 2013, MNRAS, 435, 1928
Peebles P. J. E., 2000, ApJ, 534, L127
Peter A. H. G., Rocha M., Bullock J. S., Kaplinghat M., 2013, MNRAS, 430, 105
Pfrommer C., Chang P., Broderick A. E., 2012, ApJ, 752, 24
Planck Collaboration XVI, 2014, A&A, 571, A16
Polisensky E., Ricotti M., 2011, Phys. Rev. D, 83, 043506
Pontzen A., Governato F., 2012, MNRAS, 421, 3464
Randall L., Scholtz J., 2015, J. Cosmol. Astropart. Phys., 9, 057
Rocha M., Peter A. H. G., Bullock J. S., Kaplinghat M., Garrison-Kimmel S., Oñorbe J., Moustakas L. A., 2013, MNRAS, 430, 81
Sawala T., Scannapieco C., White S., 2012, MNRAS, 420, 1714
Sawala T. et al., 2016, MNRAS, 457, 1931
Schaller M., Robertson A., Massey R., Bower R. G., Eke V. R., 2015, MNRAS, 453, L58
Schewtschenko J. A., Wilkinson R. J., Baugh C. M., Boehm C., Pascoli S., 2015, MNRAS, 449, 3587
Schive H.-Y., Chiueh T., Broadhurst T., 2014, Nature Phys., 10, 496
Schneider A., Anderhalden D., Macciò A. V., Diemand J., 2014, MNRAS, 441, L6
Seljak U., Zaldarriaga M., 1996, ApJ, 469, 437
Sigurdson K., Kamionkowski M., 2004, Phys. Rev. Lett., 92, 171302
Spergel D. N., Steinhardt P. J., 2000, Phys. Rev. Lett., 84, 3760
Spergel D. N., Flauger R., Hložek R., 2015, Phys. Rev. D, 91, 023518
Springel V., 2005, MNRAS, 364, 1105
Springel V., 2010, MNRAS, 401, 791
Van den Aarssen L. G., Bringmann T., Pfrommer C., 2012, Phys. Rev. Lett., 109, 231301
Vegetti S., Vogelsberger M., 2014, MNRAS, 442, 3598
Viel M., Becker G. D., Bolton J. S., Haehnelt M. G., 2013, Phys. Rev. D, 88, 043502
Villaescusa-Navarro F., Dalal N., 2011, J. Cosmol. Astropart. Phys., 3, 24
Vogelsberger M., Zavala J., 2013, MNRAS, 430, 1722
Vogelsberger M., Zavala J., Loeb A., 2012, MNRAS, 423, 3740
Vogelsberger M., Zavala J., Simpson C., Jenkins A., 2014a, MNRAS, 444, 3684
Vogelsberger M. et al., 2014b, Nature, 509, 177
Walker M. G., Peñarrubia J., 2011, ApJ, 742, 20
Wang J., White S. D. M., 2007, MNRAS, 380, 93
Wang J., Frenk C. S., Navarro J. F., Gao L., Sawala T., 2012, MNRAS, 424, 2715
Wang W., Han J., Cooper A. P., Cole S., Frenk C., Lowing B., 2015, MNRAS, 453, 377
Weisz D. R., Dolphin A. E., Skillman E. D., Holtzman J., Gilbert K. M., Dalcanton J. J., Williams B. F., 2014, ApJ, 789, 147
Wolf J., Martinez G. D., Bullock J. S., Kaplinghat M., Geha M., Muñoz R. R., Simon J. D., Avedo F. F., 2010, MNRAS, 406, 1220
Zavala J., Jing Y. P., Faltenbacher A., Yepes G., Hoffman Y., Gottlöber S., Catinella B., 2009, ApJ, 700, 1779
Zavala J., Vogelsberger M., Walker M. G., 2013, MNRAS, 431, L20

This paper has been typeset from a TEX/LATEX file prepared by the author.